Molecular Catalysis 565 (2024) 114387

Contents lists available at ScienceDirect

Molecular Catalysis

journal homepage: www.journals.elsevier.com/molecular-catalysis

Directly accessing the alkyne-aldehyde-amine (A^3) coupling catalytic cycle using molecular gold(I) acetylide complexes for synthesizing propargylamines and amino indolizines

Jyoti Singh [1], Purva Dua [1], Gopalan Rajaraman [*], Prasenjit Ghosh [*]

Department of Chemistry, Indian Institute of Technology Bombay, Powai, Mumbai 400 076, India

A R T I C L E I N F O

Keywords:
Acyclic aminooxy carbene (AAOC)
Gold(I)
Acetylide
Alkyne
Amine
Aldehyde
A^3 coupling
Propargylamine
Indolizine
DFT studies
Non-covalent Au
H–C interaction

A B S T R A C T

The gold(I) acetylide complexes of Acyclic Aminooxy Carbene (AAOC) ligands, [{(4-R^1-2,6-*t*-Bu_2-C_6H_2O)(NCy_2)}methylidene]Au[C≡C(*p*-$C_6H_4R^2$)] [where R^1 = H; R^2 = H (**1**), and R^1 = *t*-Bu; R^2 = H (**4**)] efficiently catalyzed the three-component Alkyne-Aldehyde-Amine (A^3) coupling yielding propargylamine and amino indolizine compounds, thereby implicating its direct role in the catalytic cycle. The DFT studies performed on a simplified gold(I) precatalyst, [{(2,4,6-Me_3-C_6H_2O)(NCy_2)}methylidene]Au[C≡CPh] (**4'**), at B3LYP-D3/def2-TZVP of theory implicated the role of non-covalent Au•••H–C interactions in the A^3 coupling reactions producing propargylamine and subsequently amino indolizine *via* intramolecular cyclization of propargylamine followed by an intramolecular 1,2-hydrogen transfer-step for the 2-formylpyridine substrate. The non-covalent Au•••H–C (alkyl) and Au•••H–C(aryl) interactions participate in tandem to influence the overall reaction kinetic barrier, and thereby illustrating the importance of such interactions in gold catalysis. The gold(I) acetylide complexes, [{(4-R^1-2,6-*t*-Bu_2-C_6H_2O)(NCy_2)}methylidene]Au[C≡C(*p*-$C_6H_4R^2$)] [where R^1 = H; R^2 = H (**1**), Me (**2**), OPh (**3**): R^1 = *t*-Bu; R^2 = H (**4**), Me (**5**), OPh (**6**)] were conveniently synthesized from the corresponding chloro analogues [{(4-R^1-2,6-*t*-Bu_2-C_6H_2O)(NCy_2)}methylidene]AuCl (where R^1 = H, *t*-Bu) by the treatment with terminal alkyne HC≡C(*p*-$C_6H_4R^2$) (where R^2 = H, Me, OPh) in the presence of K_2CO_3 as a base in *ca.* 88−95 % yield.

Introduction

Transition metal acetylides store a rich and diverse chemistry through a gamut of stoichiometric, sub-stoichiometric, and catalytic transformations, paving the way for the utilization of the acetylene-based C_2-feedstocks [1,2]. Consequently, the transition metal acetylides are active intermediates [3] in many important catalytic processes, namely Castro–Stephens reaction [4-6], Sonagashira coupling [7-10], the alkyne-azide 1,3-dipolar cycloaddition reactions [11-15], cross-coupling of diazo compounds with terminal alkynes [16-18], carboxylation and carboxylative coupling reactions of terminal alkynes [19-22], metal acetylide-diazocarbonyl compound cycloaddition reactions [3,23-25], azomethine imine–alkyne cycloaddition reactions [25,26], alkynylation of azomethine imine reactions [27], Kinugasa reactions [28-30], the Alkyne-Aldehyde-Amine (A^3) coupling [31], and etc. giving a wide variety of organic compounds of both industrial and pharmaceutical interests alike [32,33]. The synthesis-related challenges associated with the extreme sensitivities of the organometallic transition metal acetylides toward air, moisture, and temperature make their study demanding. In most instances, the exploration and expansion of the chemistry of the transition metal acetylides has been achieved through the *in-situ* generation of the metal acetylide species during the course of the reaction [32,33]. Hence, direct synthesis of the relevant well-defined molecular transition metal acetylide complexes and their corresponding application studies has significantly lagged behind the aforementioned and more convenient *in-situ* generation studies. Subscribing to this line of rationale, we decided to employ well-defined molecular metal acetylide complexes for those specific catalytic applications that contain metal-acetylide as an active intermediate species in its catalytic cycle. The direct entry to the catalytic cycle *via* the catalytically active metal-acetylide intermediate would provide an up close and insightful perspective on the catalyst mode of action.

* Corresponding author.
E-mail addresses: jyotisingh@iitb.ac.in (J. Singh), 194033052@iitb.ac.in (P. Dua), rajaraman@chem.iitb.ac.in (G. Rajaraman), pghosh@chem.iitb.ac.in (P. Ghosh).

[1] J. S. and P. D. contributed equally to this work.

https://doi.org/10.1016/j.mcat.2024.114387
Received 16 April 2024; Received in revised form 2 July 2024; Accepted 9 July 2024
Available online 20 July 2024
2468-8231/© 2024 Elsevier B.V. All rights are reserved, including those for text and data mining, AI training, and similar technologies.

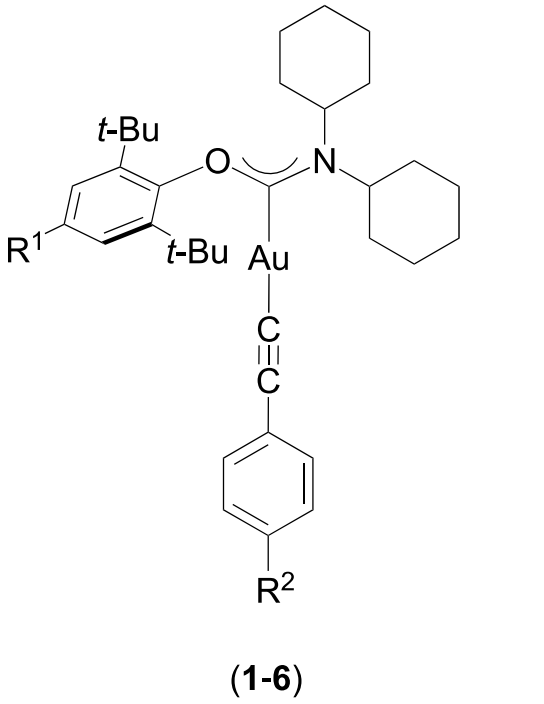

Fig. 1. Gold(I) acetylide derivatives (**1**−**6**) stabilized by acyclic aminooxy carbene (AAOC).

The Alkyne-Aldehyde-Amine (A^3) coupling provides a direct convenient access to the propargylamine core, that is common to many drugs and pharmaceutically important compounds like, Seleginine [34-36] and Rasagiline [37], used in the treatment of early symptoms of the Parkinson's disease, and Ladostigil [38,39], used as a neuroprotective agent. The three-component (A^3) coupling also provides a direct synthetic route to the nitrogen-containing heterocycles, like, indolizines, which are of interest for their potential bioactive properties. With our interest in tandem and multi-component reactions [40-46] in line with our efforts in understanding the utility of the transition metal complexes of the heteroatom stabilized singlet carbene complexes in catalytic and biomedical applications [47,48], we decided to study the Alkyne-Aldehyde-Amine (A^3) coupling by directly accessing the catalytic cycle through the metal-acetylide intermediate of its catalytic cycle. For this purpose, we desired to employ well-defined gold(I) acetylide molecular complexes of the acyclic aminooxy carbene (AAOC) ligands in the Alkyne-Aldehyde-Amine (A^3) coupling reaction.

The theoretical investigations of several noble metals like Au and Ag-mediated A^3 coupling reactions reveal the prominent role of the Au•••H–C(alkyl) and Au•••H–C(aryl) interactions in influencing the overall reaction rate significantly [49-52]. Though considerable insights are available on the A^3 coupling mechanism [53], similar understanding of the tandem A^3 coupling/cyclization reaction forming heterocycles has not been established yet. Hence in the current study, we intend to explore the mechanisms of the A^3 coupling and the tandem A^3 coupling/cyclization reaction and also probe the influence of the non-covalent interactions in these catalytic cycles. In particular, using comprehensive computational study, we aim to look into the influence of the non-covalent Au•••H–C(alkyl) and Au•••H–C(aryl) interactions in the A^3 coupling and the tandem A^3 coupling/cyclization reactions from the prisim of their catalytic pathways.

Here in the manuscript, we report Alkyne-Aldehyde-Amine (A^3) coupling reaction by directly entering the catalytic cycle at its metal-acetylide intermediate with well-defined gold(I)-acetylide acyclic aminooxy carbene (AAOC) complexes (Fig. 1). Specifically, the representative [{(4-R^1-2,6-*t*-Bu_2-C_6H_2O)(NCy_2)}methylidene]Au[C≡C(*p*-$C_6H_4R^2$)] [where R^1 = H; R^2 = H (**1**), and R^1 = *t*-Bu; R^2 = H (**4**),)] complexes efficiently catalyzed Alkyne-Aldehyde-Amine (A^3) coupling producing propargylamines and amino indolizines, and in the process attesting to the direct involvement of the metal acetylide moiety in the catalysis reaction. The DFT studies provide valuable mechanistic insights on the catalyst mode of action.

Results and Discussions

The gold(I) acetylide complexes, [{(4-R^1-2,6-*t*-Bu_2-C_6H_2O)(NCy_2)} methylidene]Au[C≡C(*p*-$C_6H_4R^2$)] [where R^1 = H; R^2 = H (**1**), Me (**2**), OPh (**3**): R^1 = *t*-Bu; R^2 = H (**4**), Me (**5**), OPh (**6**)], were synthesized from the chloro derivatives, [{(4-R^1-2,6-*t*-Bu_2-C_6H_2O)(NCy_2)}methylidene] AuCl (where R^1 = H, *t*-Bu) [46] by reaction with terminal alkynes, namely, phenylacetylene, 4-ethynyltoluene and 1-ethynyl-4-phenoxybenzene, in the presence of K_2CO_3 as a base in CH_2Cl_2, in *ca.* 88−95 % yields using literature procedure (Scheme 1) [54-56]. The $^{13}C\{^1H\}$ NMR showed a significant downfield shift of the characteristic Au(I)−$\underline{C}_{carbene}$ resonance at δ *ca.* 227.5-227.9 ppm for the gold(I) acetylide (**1**−**6**) complexes (Supporting Information Figures S9, S10, S16, S17, S23, S24, S30, S31, S37, S38, S44 and S45) and compared well that reported for the related acyclic diamino carbene (ADC) based analogues

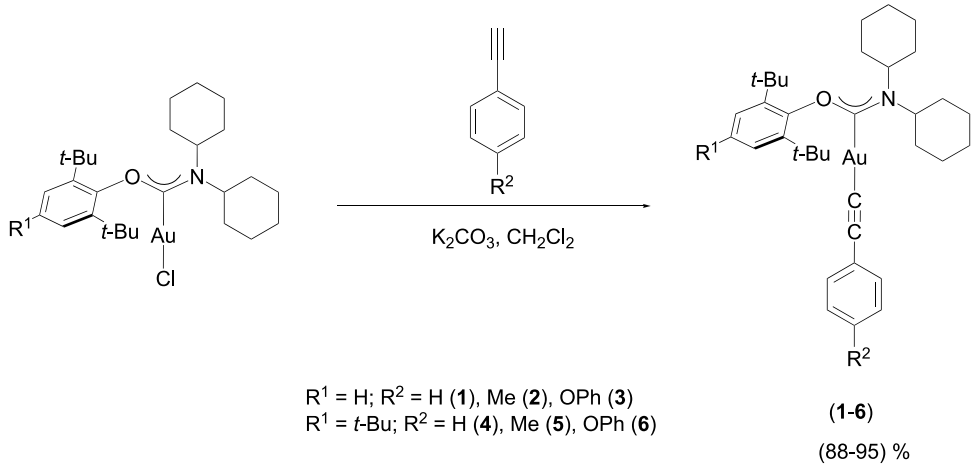

Scheme 1. Synthesis route to the acyclic aminooxy carbene (AAOC) stabilized gold(I) acetylide derivatives (**1**−**6**).

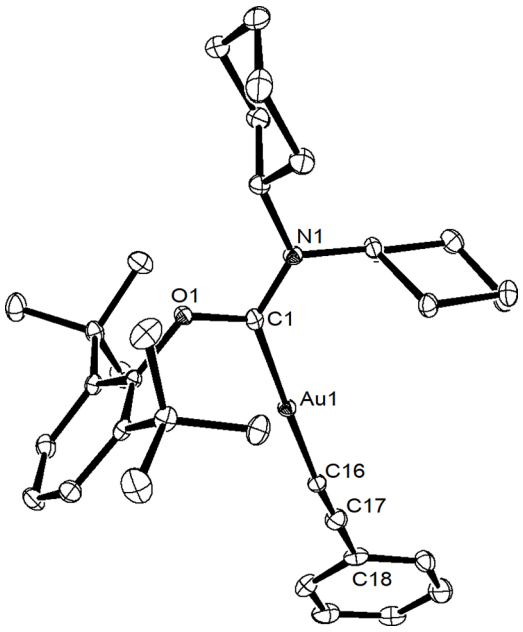

Fig. 2. ORTEP of **1** with thermal ellipsoids drawn at the 50 % probability level. Hydrogen atoms and solvent $CHCl_3$ are omitted for clarity. Selected bond lengths (Å) and angles (°): Au(1)−C(1) 2.028(2), O(1)−C(1) 1.351(2), N(1)−C(1) 1.323(3), Au(1)−C(16) 2.002(2), C(16)−C(17) 1.196(3), N(1)−C(1)−O(1) 111.12(17), N(1)−C(1)−Au(1) 126.99(14), O(1)−C(1)−Au(1) 121.71(13), C(1)-Au(1)-C(16) 174.15(7), Au(1)−C(16)−C(17) 172.13(18).

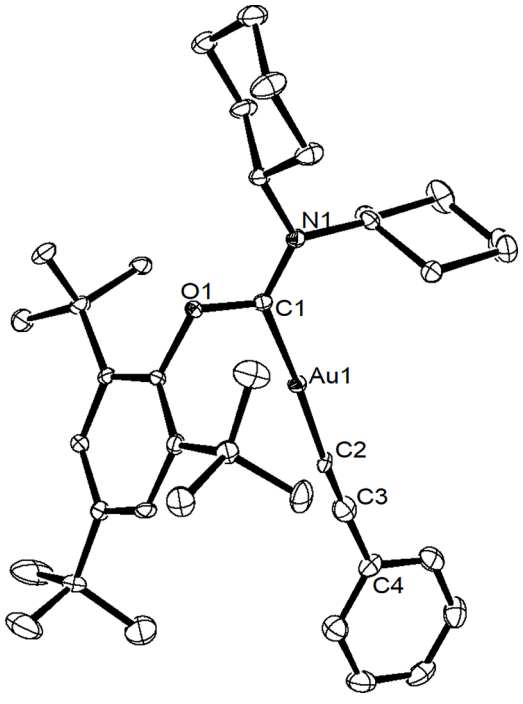

Fig. 3. ORTEP of **4** with thermal ellipsoids drawn at the 50 % probability level. Hydrogen atoms are omitted for clarity. Selected bond lengths (Å) and angles (°): Au(1)−C(1) 2.043(3), O(1)−C(1) 1.363(4), N(1)−C(1) 1.318(4), Au(1)−C(2) 2.018(3), C(2)−C(3) 1.176(4), N(1)−C(1)−O(1) 112.0(2), N(1)−C(1)−Au(1) 129.6(2), O(1)−C(1)−Au(1) 118.40(19), C(1)-Au(1)-C(2) 177.25(11), Au(1)−C(2)−C(3) 173.8(3).

namely, [{(NEt_2)(NH*t*-Bu)}methylidene]Au(C≡CCH_3) (206.4 ppm) [57], [{(NEt_2)(NH*t*-Bu)}methylidene]Au(C≡C(*p*-$C_6H_4NO_2$)) (204.7 ppm) [58], [[{(NEt_2)(NH*t*-Bu)}methylidene]Au]$_2$(μ-1,2-(C≡C)$_2C_6Me_4$) (206.9 ppm) [59], [[{(NEt_2)(NH*t*-Bu)}methylidene]Au]$_2$(μ-1,3-(C≡C)$_2C_6H_4$) (205.4 ppm) [60] (Supporting Information Table S2). Similarly, in the $^{13}C\{^1H\}$ NMR, the Au[C≡C(*p*-$C_6H_4R^2$)] (where R^2 = H, Me, OPh) resonance appeared at *δ ca.* 121.4-124.2 ppm for the (**1**−**6**) complexes (Supporting Information Figures S9, S10, S16, S17, S23, S24, S30, S31, S37, S38, S44 and S45) and were considerable upfield shifted by (Δδ) *ca.* 2.4 ppm with respect to the reported gold(I) acetylide acyclic diamino carbene (ADC) complexes namely, [{(NEt_2)(NH*t*-Bu)}methylidene]Au(C≡CCH_3), (114.6 ppm) [57], [{(NEt_2)(NH*t*-Bu)}methylidene]Au(C≡C(*p*-$C_6H_4NO_2$)), (133.5 ppm) [58], [[{(NEt_2)(NH*t*-Bu)}methylidene]Au]$_2$(μ-1,2-(C≡C)$_2C_6Me_4$), (126.6 ppm) [59], and [[{(NEt_2)(NH*t*-Bu)}methylidene]Au]$_2$(μ-1,3-(C≡C)$_2C_6H_4$), (126.0 ppm) [60]. Furthermore, the IR ν(C≡C) stretching for the Au[C≡C(*p*-$C_6H_4R^2$)] (where R^2 = H, Me, OPh) moiety appeared at 2107 cm^{-1} (**1**), 2116 cm^{-1} (**2**), 2113 cm^{-1} (**3**), 2117 cm^{-1} (**4**), 2118 cm^{-1} (**5**) and 2119 cm^{-1} (**6**) frequencies (Supporting Information Figures S11, S18, S25, S32, S39 and S46) in agreement with their acyclic diamino carbene (ADC) analogs (Supporting Information Table S2).

The molecular structures of the (**1**−**6**) complexes revealed their discrete monomeric nature, with a two-coordinated linear gold(I) center flanked on its sides by the acyclic aminooxy carbene (AAOC) ligand and the [C≡C(*p*-$C_6H_4R^2$)] (where R^2 = H, Me, OPh) moiety. The Au−$C_{carbene}$ bond distances of 2.028(2) Å (**1**), 2.062(5) Å (**2**), 2.038(2) Å (**3**), 2.043 (3) Å (**4**), 2.040(3) Å (**5**) and 2.039(3) Å (**6**) (Figs. 2, 3 and Supporting Information Figures S1, S2, S3 and S4 and Table S1) are shorter than the sum of their individual covalent radii [$d(C^2_{sp}$−Au) = 2.09 Å] [61]. The (**1**−**6**) complexes exhibit bond lengths comparable to structurally characterized analogs, representatively, [{(NEt_2)(NH*t*-Bu)}methylidene]Au(C≡CCH_3) [2.045(4) Å] [57], [{(NEt_2)(NH*t*-Bu)}methylidene]Au(C≡C(*p*-$C_6H_4NO_2$)) [2.044(5) Å] [58]. [{(NEt_2)(NH*t*-Bu)}methylidene]Au{C≡C(*p*-C_6H_4-((*E*)-CH=$CHC_6H_4NO_2$))} [2.052(6) Å] [58], [[{(NEt_2)(NH*t*-Bu)}methylidene]Au]$_2$(μ-1,2-(C≡C)$_2C_6Me_4$) [2.046(3) Å] [59] and [[{(NEt_2)(NH*t*-Bu)}methylidene]Au]$_2$(μ-1,3-(C≡C)$_2C_6H_4$) [2.043(4) Å] [60] (Supporting Information Table S2). Likewise, the Au−$C_{acetylide}$ bond distances of 2.002(2) Å (**1**), 1.998(5) Å (**2**), 1.995(2) Å (**3**), 2.018(3) Å (**4**), 1.992(3) Å (**5**) and 1.986(4) Å (**6**) (Figs. 2, 3 and Supporting Information Figures S1, S2, S3 and S4 and Table S1) are also shorter than the sum of their individual covalent radii [$d(C_{sp}$−Au) = 2.05 Å] [61] and are in agreement with related examples (Supporting Information Table S2). The C≡C bond distances of 1.196(3) Å (**1**), 1.229 (8) Å (**2**), 1.203(3) Å (**3**), 1.176(4) Å (**4**), 1.196(4) Å (**5**) and 1.204(5) Å (**6**) (Figs. 2, 3 and Supporting Information Figures S1, S2, S3 and S4 and Table S1) are also shorter than the sum of their individual covalent radii [*d*(C≡C) = 1.38 Å] [61].

Significantly enough, all the gold(I) acetylide (**1**−**6**) complexes successfully catalyzed the A^3-coupling of the representative substrates, formaldehyde, phenylacetylene and morpholine at 80 °C and 0.5 mol % of the catalyst loadings yielding the propargylamine (**7**) in quantitative yields of 93 % for (**1**), 98 % for (**2**), 96 % for (**3**), 96 % for (**4**), 99 % for (**5**) and 98 % for (**6**) (Table 1).

With the intent of demonstrating the entry to the catalytic cycle through its metal-acetylide intermediate, the following two representative gold(I) acetylide complexes, [{(4-R^1-2,6-*t*-Bu_2-C_6H_2O)(NCy_2)}methylidene]Au[C≡C(*p*-$C_6H_4R^2$)], where R^1 = H, R^2 = H (**1**) and R^1 = *t*-Bu, R^2 = H (**4**), were explored in the A^3-coupling reaction of Alkyne-Aldehyde-Amine for the preparation of the propargylamines derivatives. Furthermore, in order to compare the catalytic activities of the gold(I) acetylide (**1**) and (**4**) complexes with that of accessing the same A^3-coupling catalytic cycle, through its other metal-chloro catalytic intermediate, the corresponding chloro complexes, [{(2,6-*t*-Bu_2-C_6H_3O)(NCy_2)}methylidene]AuCl and [{(2,4,6-*t*-Bu_3-C_6H_2O)(NCy_2)}methylidene]AuCl, were also employed in the A^3-coupling reaction. Significantly enough, both the gold(I) acetylide intermediates, (**1**) and (**4**), and their corresponding chloro derivatives carried out the A^3-coupling reaction for a variety of aldehyde, amine, and terminal alkyne substrates with equal efficiency and thereby implicating the gold(I) acetylide and

Table 1
Selected results for the propargylamine synthesis catalysed by the Au(I) acetylide (**1**−**6**) complexes for the representative substrates namely, formaldehyde, phenylacetylene and morpholine.[a]

(**7**)

entry	catalyst	yield[b]
1.	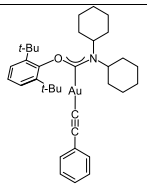 (**1**)	93
2.	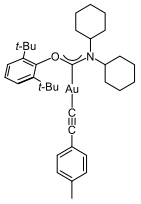 (**2**)	98
3.	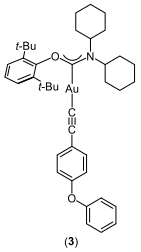 (**3**)	96
4.	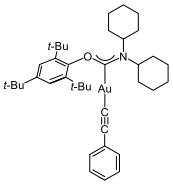 (**4**)	96
5.	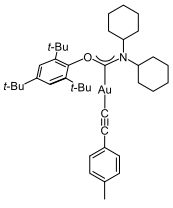 (**5**)	99
6.	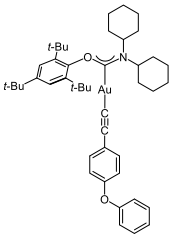 (**6**)	98

Reaction conditions: (a). 1:1.2:4 ratio of phenylacetylene: morpholine: formaldehyde and 0.5 mol % of catalysts loading; 2 mL of CH_3CN at 80 °C for the 24 hours. (b). Isolated yields (%).

Table 2
Selected results for the synthesis of propargylamine by coupling of terminal alkyne, amine and aldehyde catalyzed by the representative catalysts (**1**), (**4**), [{(2,6-*t*-Bu_2-C_6H_3O)(NCy_2)}methylidene]AuCl [46] and [{(2,4,6-*t*-Bu_3-C_6H_2O)(NCy_2)}methylidene]AuCl complexes [46].[a]

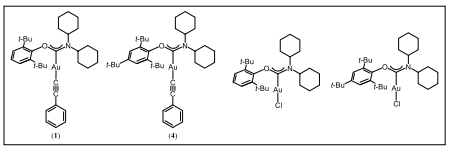

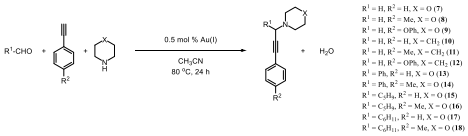

entry	reagent	reagent	reagent	product	(**1**) yield[b]	yield[b]	(**4**) yield[b]	yield[b]
1.	HCHO			(**7**)	93	99	96	96
2.	HCHO			(**8**)	98	95	98	99
3.	HCHO			(**9**)	99	96	95	96
4.	HCHO			(**10**)	94	89	96	87
5.	HCHO			(**11**)	95	96	98	95
6.	HCHO			(**12**)	93	94	95	93
7.				(**13**)	19	15	43	18
8.				(**14**)	36	35	47	43
9.				(**15**)	54	52	55	54
10.				(**16**)	63	69	73	70
11.				(**17**)	80	79	78	85
12.				(**18**)	85	91	93	88

Reaction conditions: (a). 1:1.2:4 ratio of terminal alkynes: *sec* amine: formaldehyde and 1:1.2:1.2 ratio of terminal alkynes: *sec* amine: benzaldehyde/cyclohexanecarboxaldehyde/cyclopentanecarboxaldehyde; 0.5 mol % of catalyst (**1**), (**4**), [{(2,6-*t*-Bu_2-C_6H_3O)(NCy_2)}methylidene]AuCl and [{(2,4,6-*t*-Bu_3-C_6H_2O)(NCy_2)}methylidene]AuCl; 2 mL of CH_3CN at 80 °C for the 24 hours. (b). Isolated yields (%).

gold(I) chloro species to be part of the same catalytic cycle. Detailed optimization studies along with control and blank experiments were undertaken to arrive at the catalysis conditions (Supporting Information Table S4 and S5).

In particular, all the gold(I) acetylide (**1**) and (**4**) and gold(I) chloro complexes, [{(2,6-*t*-Bu_2-C_6H_3O)(NCy_2)}methylidene]AuCl and [{(2,4,6-*t*-Bu_3-C_6H_2O)(NCy_2)}methylidene]AuCl, performed the A^3-coupling at 80 °C at 0.5 mol % of the catalyst loading in 15−99 % yielding. For example, the coupling of formaldehyde, phenylacetylene and morpholine proceeds in 93 % for (**1**) and 96 % for (**4**), the gold(I) acetylide complexes. The corresponding yields for the chloro derivatives are 99 % and 96 % respectively (Table 2). Additionally, no meaningful differences were observed in the product yields are observed for the gold(I) acetylide (**1**) and (**4**) complexes as well for the corresponding gold(I) chloro

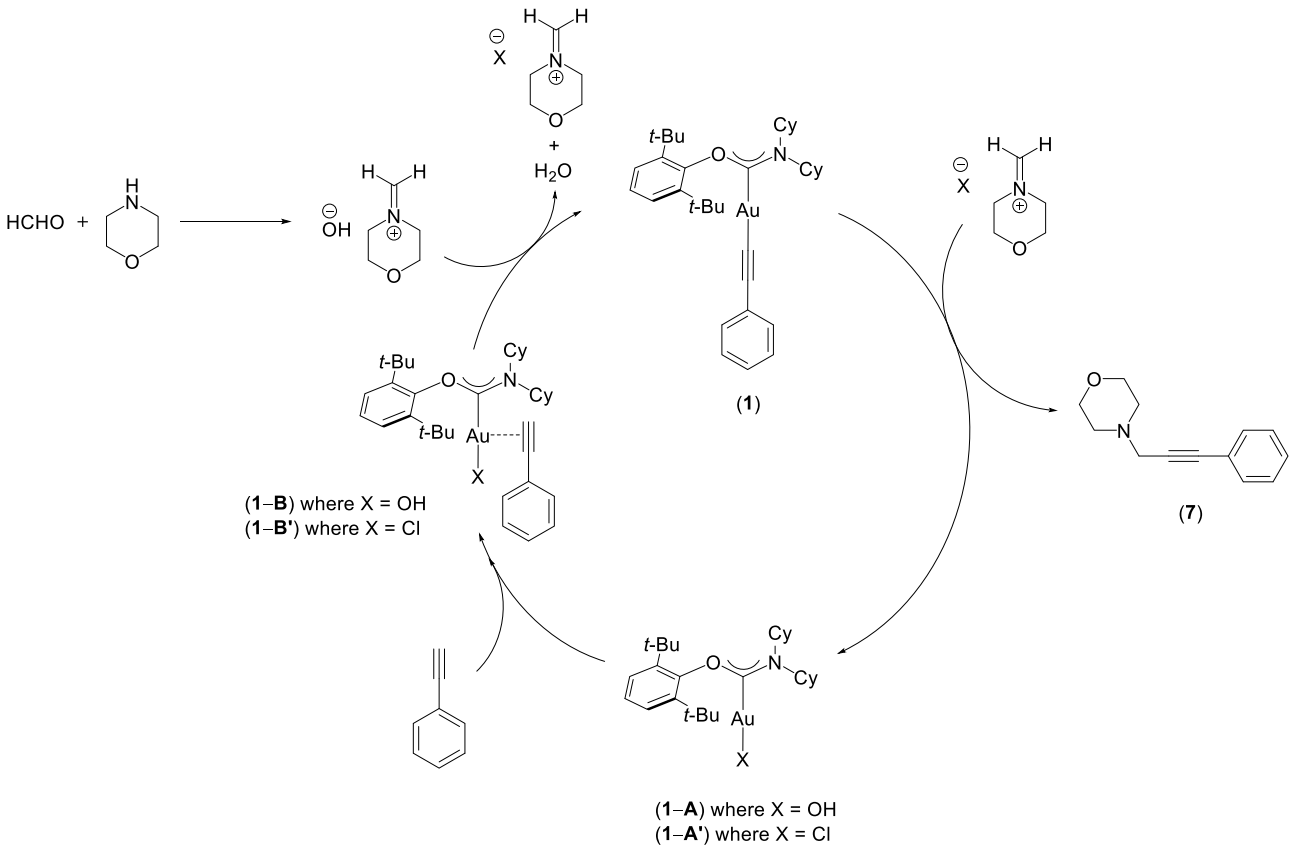

Scheme 2. Proposed mechanism for the Au(I) acyclic aminooxy carbene (AAOC) (**1**) catalyzed the synthesis of propargylamine by coupling of the representative substrates namely, phenylacetylene, formaldehyde and morpholine.

derivatives, [{(2,6-*t*-Bu_2-C_6H_3O)(NCy_2)}methylidene]AuCl and [{(2,4,6-*t*-Bu_3-C_6H_2O)(NCy_2)}methylidene]AuCl, suggesting all four complexes equally active in partaking the coupling reaction. The superiority of the acyclic aminooxy carbene (AAOC) ligand in the coupling reaction is evident from the observation of higher yields obtained in case of the gold(I) acetylide (**1**) [93 %] and (**4**) [96 %] complexes and the chloro derivatives [{(2,6-*t*-Bu_2-C_6H_3O)(NCy_2)}methylidene]AuCl [99 %] and [{(2,4,6-*t*-Bu_3-C_6H_2O)(NCy_2)}methylidene]AuCl [96 %], as compared to the following benchmark complexes namely, [1,3-*bis*(mesityl)imidazol-2-ylidene]AuCl [62] [84 %] (entry 8 and Supporting Information, Table S5) and [1,3-*bis*(2,6-diisopropylphenyl)imidazol-2-ylidene]AuCl [62] [92 %] (entry 9 and Supporting Information Table S5) for the coupling of phenylacetylene, formaldehyde and morpholine. Substrate scope explored with different aldehydes derivatives namely, formaldehyde, benzaldehyde, cyclopentanecarboxaldehyde, cyclohexanecarboxaldehyde along with a variety of terminal alkynes such as phenylacetylene, 4-ethynyltoluene, and 1-ethynyl-4-phenoxybenzene and cyclic secondary amines, morpholine, and piperidine, showed higher yields of *ca.* 52−99 % for formaldehyde, cyclohexanecarboxaldehyde, cyclopentanecarboxaldehyde, but lower yields of *ca.* 15−47 % for the benzaldehyde substrate for all of the (**1**), (**4**), [{(2,6-*t*-Bu_2-C_6H_3O)(NCy_2)}methylidene]AuCl and [{(2,4,6-*t*-Bu_3-C_6H_2O)(NCy_2)}methylidene]AuCl complexes.

In the absence of any report of A^3-coupling with a gold(I) acyclic aminooxy carbene (AAOC) complex, a comparison is made with related well-defined molecular complexes namely, [1-(methyl)-3-(2-methoxy-2-phenylethyl)imidazol-2-ylidene]AuCl [63] that exhibited *ca.* 88 % product yield at 3 mol % catalyst loading at 80 °C for 6 hours under solvent-free conditions, while [2,6-*bis*-(1-(1S)-menthyl-3-methylene-imidazol-2-ylidene)-pyridine]Au_2Cl_2 [64] displayed *ca.* 48 % product yield at 2 mol % of catalyst loading at 30 °C for 24 hours in CH_2Cl_2 for the formaldehyde, phenylacetylene and piperidine substrates. Higher yields were observed for the gold(I) acetylide (**1**) [94 %] and (**4**) [96 %] and gold(I) chloro complexes, [{(2,6-*t*-Bu_2-C_6H_3O)(NCy_2)}methylidene]AuCl [89 %] and [{(2,4,6-*t*-Bu_3-C_6H_2O)(NCy_2)}methylidene]AuCl [87 %], for the A^3-coupling of same substrates at 0.5 mol % of the catalyst loading at 80 °C for 24 hours of reaction time (Supporting Information Table S3). Here again, the catalytic superiority of the acyclic aminooxy carbene (AAOC) stabilized gold(I) acetylide (**1**) and (**4**) and gold(I) chloro complexes, [{(2,6-*t*-Bu_2-C_6H_3O)(NCy_2)}methylidene]AuCl and [{(2,4,6-*t*-Bu_3-C_6H_2O)(NCy_2)}methylidene]AuCl are underscored in A^3-coupling.

A proposed catalytic pathway for the representative gold(I) acetylide (**1**) complex initiates with an attack of the gold(I) bound acetylide moiety to the protonated morpholine imine salt, 4-methylenemorpholin-4-ium hydroxide/chloride, to eliminate the product propargylamine (**7**) along with the formation of [[{(2,6-*t*-Bu_2-C_6H_3O)(NCy_2)}methylidene]AuX] [where X = OH (**1**−**A**), Cl (**1**−**A'**)]) (Scheme 2 and Supporting Information Schemes S1 and S2). The coordination of phenylacetylene to (**1**−**A**)/(**1**−**A'**) yields the gold(I) bound phenylacetylene species, [[{(2,6-*t*-Bu_2-C_6H_3O)(NCy_2)}methylidene]AuX(HC≡CPh)], [where X = OH (**1**−**B**), Cl (**1**−**B'**)]. Subsequent reaction of (**1**−**B**)/(**1**−**B'**) with the protonated morpholine imine salt, 4-methylenemorpholin-4-ium hydroxide, regenerating the gold(I) acetylide (**1**) complex, along with the generation of the protonated morpholine imine salt, 4-methylenemorpholin-4-ium chloride, with water. Significantly enough, both of the catalytic intermediates, (**1**) and (**1**−**B'**), have been characterized by mass spectroscopy (Figs. 4 and 5 and Supporting Information Figures S117−S120).

The X-ray photoelectron spectroscopy (XPS) studies unequivocally corroborated the gold(I) mediated A^3-coupling in the synthesis of propargylamines. Specifically, under all the following conditions, *i.e.* the XPS experiments when performed (*i*) only with the precatalyst (**4**), (*ii*) the precatalyst (**4**) mixed with benzaldehyde and morpholine at room

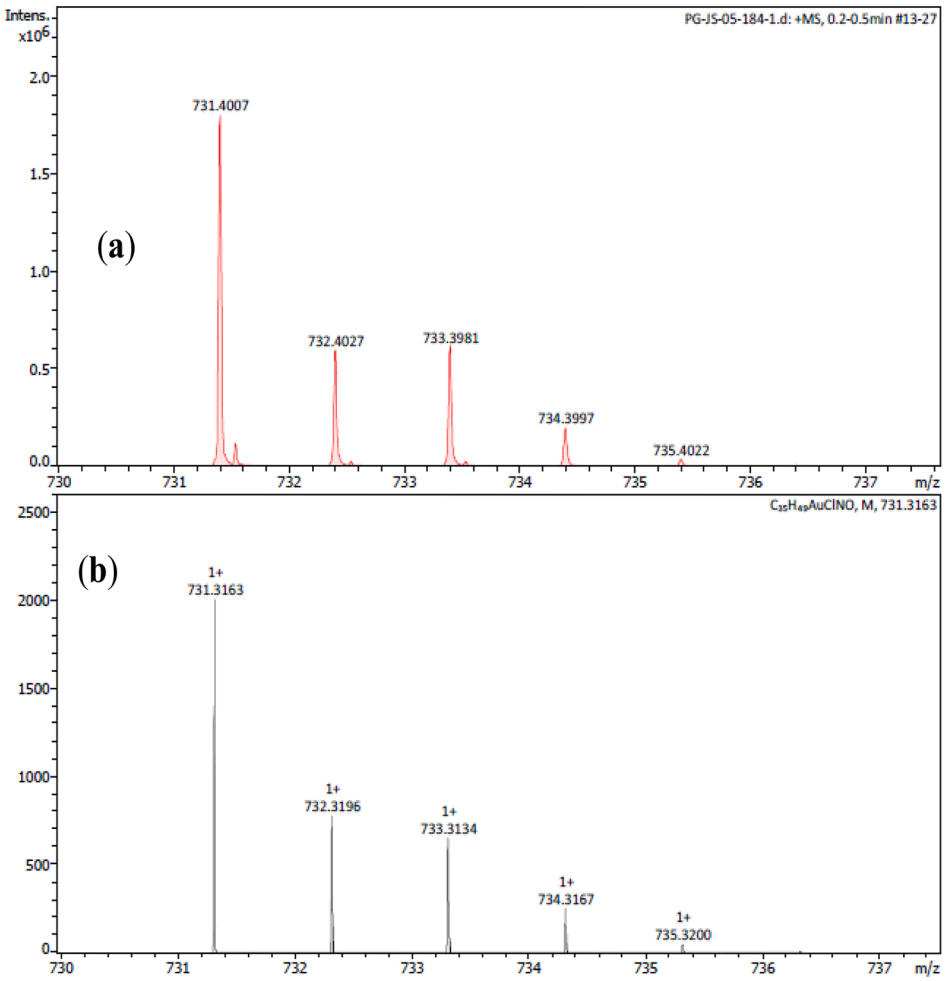

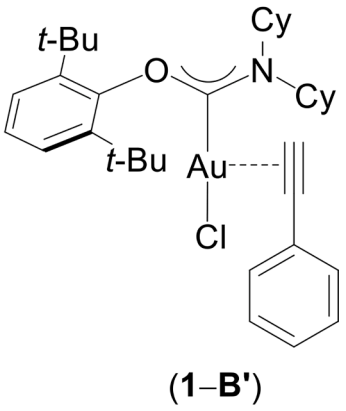

(1–B')

Fig. 4. ESI−MS data of the {[{(2,6-*t*-Bu_2-C_6H_3O)(NCy_2)}methylidene]AuCl(HC≡CPh)} species (**1**−**B'**), detected in the reaction mixture of 0.5 mol % catalyst [{(2,6-*t*-Bu_2-C_6H_3O)(NCy_2)}methylidene]AuCl and phenylacetylene (1.00 mmol), *ca.* 2 mL of CH_3CN at room temperature. [(a) Experimental and (b) simulated pattern of ESI−MS data].

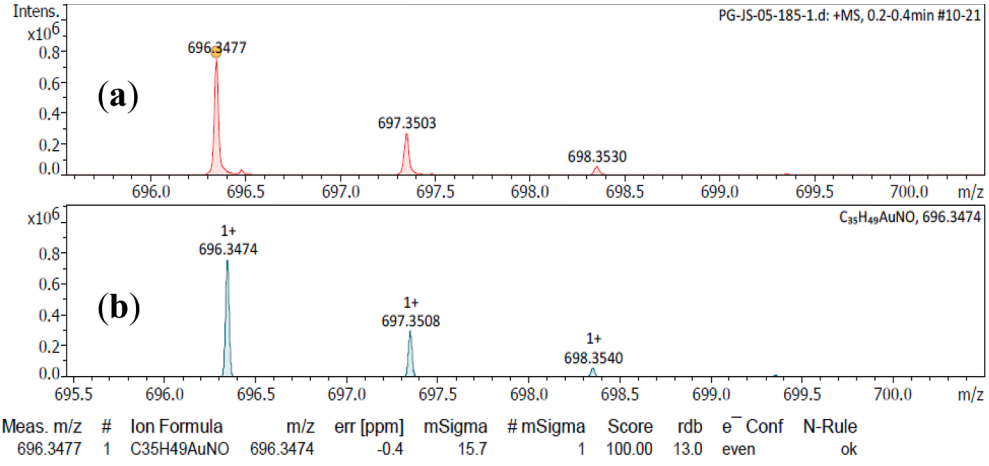

Meas. m/z	#	Ion Formula	m/z	err [ppm]	mSigma	# mSigma	Score	rdb	e⁻ Conf	N-Rule
696.3477	1	C35H49AuNO	696.3474	-0.4	15.7	1	100.00	13.0	even	ok

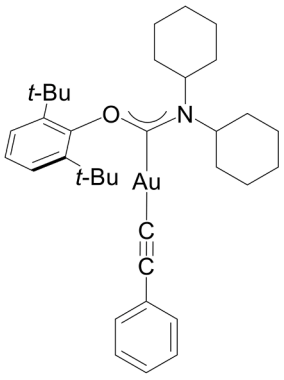

(1)

Fig. 5. HRMS data of the {[{(2,6-*t*-Bu_2-C_6H_3O)(NCy_2)}methylidene]Au(C≡CPh)} species (**1**), detected in the reaction mixture of 0.5 mol % catalyst [{(2,6-*t*-Bu_2-C_6H_3O)(NCy_2)}methylidene]AuCl, phenylacetylene (1.00 mmol), formaldehyde (1.20 mmol) and morpholine (1.20 mmol), *ca.* 2 mL of CH_3CN at room temperature. [(a) Experimental and (b) simulated pattern of ESI−MS data].

temperature for 5 minutes, and (*iii*) the precatalyst (**4**) under catalysis conditions in presence with phenylacetylene, benzaldehyde and morpholine for the 24 hours at 80 °C, produced the characteristics Au *4f* signals at two typical binding energies peaks of Au $4f_{5/2}$ at 88.5 eV and of Au $4f_{7/2}$ at 84.8 eV, in agreement with the Au (+1) oxidation state in all instances [65-68]. (Fig. 6 and Supporting Information Figures S121−S123).

Propargylamines are important for their utility as crucial

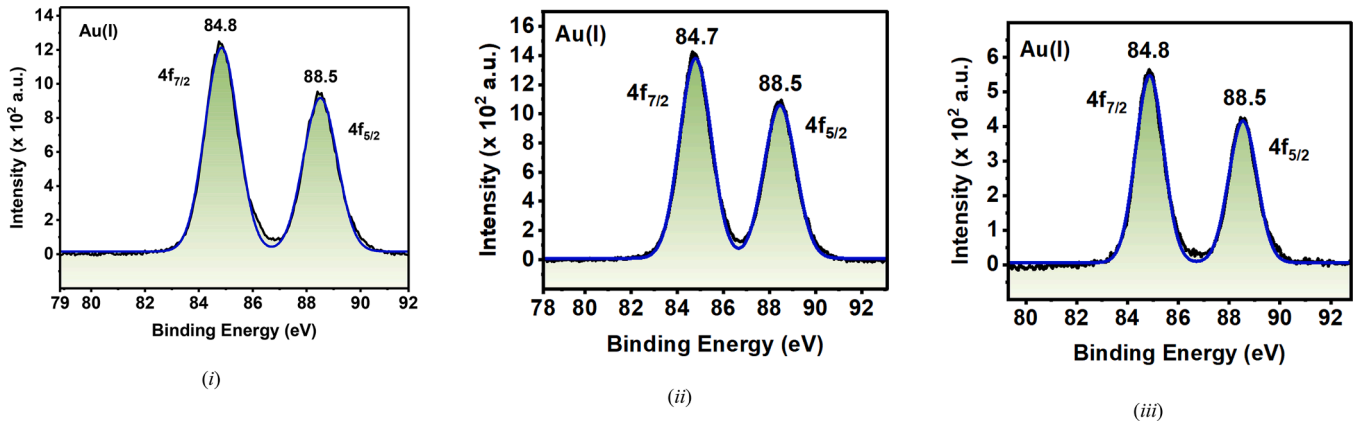

Fig. 6. XPS analysis for the Au 4f signal (*i*) the precatalyst (**4**), (*ii*) the precatalyst (**4**) with benzaldehyde and morpholine at room temperature and (*iii*) the precatalyst (**4**) with phenylacetylene, benzaldehyde and morpholine for the 24 hours at 80 °C stirring.

intermediates in the synthesis of various heterocycles common to natural products and therapeutic drugs [63,69]. Hence, the preparation of various amino indolizine compounds through propargylamine formed *via* A^3-coupling reaction represents a significant demonstration of the coupling reaction. Indeed, the two representative complexes namely, the gold(I) acetylide (**1**) complex and the gold(I) chloro [{(2,6-*t*-Bu_2-C_6H_3O)(NCy_2)}methylidene]AuCl complex, successfully produced various amino indolizine derivatives (**19**−**23**) by A^3-coupling of pyridine-2-carboxaldehyde and morpholine with several terminal alkyne derivatives namely, phenylacetylene, 4-ethynyltoluene, 1-ethynyl-4-phenoxybenzene, 1-ethynyl- 4-chlorobenzene, and 1-ethynyl-4--bromobenzene, in 41−73 % yield (Table 3 and Supporting Information Figures S97−S116). The amino indolizine derivatives (**20**) and (**23**) has also been structurally characterized revealing its expected cyclic motif.

A mechanism proposed for the preparation of the amino indolizine derivative (**19**) for the representative gold(I) acetylide (**1**) complex consists of two catalytic cycles. The first catalytic cycle proceeds by gold (I) acetylide (**1**) catalyzed A^3-coupling of pyridine-2-carboxaldehyde, morpholine and phenylacetylene yielding the corresponding propargylamine derivative that enters the second catalytic cycle by coordination to the CH_3CN bound gold(I) species (**1-C**) to give the (**1-E**) intermediate. The (**1-E**) intermediate undergoes intramolecular cyclization to produce the (**1-F**) intermediate. Subsequent reaction can occur by two possible pathways. The pathway 1 produces the (**1-G**) intermediate that on protonation eliminates the final amino indolizine product (**19**) along with the generation of CH_3CN bound gold(I) species (**1-C**) (Scheme 3 and Supporting Information Scheme S4). The pathway 2 proceeds by an 1,2-intramolecular step giving (**19**).

Density Functional Theory Studies

We conducted our theoretical calculations in the Gaussian16 suite of programs [70], employing the B3LYP-D3 functional [71,72] combined with specific basis sets (SDD for Au [73] and 6-31G* for other atoms [71,72,74,75]. To enhance accuracy, we computed single-point energies using the B3LYP-D3 functional and the def2-TZVP basis set [76]. A Gibbs free energy correction was applied to refine gas-phase electronic energies. Solvation effects were considered through the Polarizable Continuum Model (PCM) [77] with acetonitrile as the solvent. Additionally, we performed Natural Bond Orbital (NBO) analysis [78] using the same methodology. To validate our computational methods, we compared the optimised structures of acetylide complexes (**1-6**) with single-crystal X-ray diffraction data, revealing good agreement (Supporting Information, Figures S124-S129). To conduct theoretical calculations for the proposed pathway, we focused on a simplified gold(I) precatalyst, [{(2,4,6-Me_3-C_6H_2O)(NCy_2)}methylidene]Au[C≡CPh] (**4'**), which is a modified form of the complex (**4**) with *t*-Bu groups replaced by -CH_3 groups (Supporting Information Figure S130).

13C. NMR Chemical Shift Analysis

The ^{13}C NMR spectroscopic computations were conducted using ORCA 4.2.1 [79,80] software, and the initial coordinates for these calculations were derived from prior DFT calculations performed within the Gaussian16 suite of programs. The computational methodology involved the utilization of the B3LYP hybrid functional [71,72,75] in conjunction with the RIJK approximation [81]. For specific elements, the Sapporo-DKH3-DZP-2012 basis set was employed for gold transition metal [82,83], IGLO-II for carbon (C) [84,85], and DKH-def2-SVP for all other atoms (oxygen, nitrogen, and hydrogen) [76,86,87]. The relativistic effects were incorporated using DKH method as implemented in ORCA suite. This same approach was applied to ^{13}C NMR calculations for trimethylsilyl (TMS).

Notably, the computed ^{13}C NMR chemical shifts for the (**1**−**6**) compounds exhibited excellent agreement with experimentally reported values, as documented in the Supporting Information (Supporting Information, Table S6). For instance, in the case of (**1**), the experimentally determined chemical shifts, δ *ca.* 227.6 ppm for (Au−$\underline{C}_{carbene}$), δ *ca.* 124.2 ppm for (Au−$\underline{C}_{acetylide}$), and δ *ca.* 105.2 ppm for (C≡$\underline{C}$), align closely with their respective computed counterparts, δ 227.9 ppm, δ 120.7 ppm and δ 105.3 ppm. A larger deshielding of the Au−$\underline{C}_{carbene}$ observed is found to be associated with a significant contribution to the paramagnetic spin-orbit term compared to the Au−$\underline{C}_{acetylide}$ carbon shift. Particularly, the dominant contribution is nearly five times larger for the former compared to the latter. This contribution is correlated to a charge-transfer process [88], and thus it indicates the occurrence of a significant charger transfer from the carbene carbon to the Au atom, thereby resulting in the observed deshielding.

Steric Parameter (% Buried Volume) Analysis

The steric properties and buried volume (% V_{Bur}) of acetylide the (**1**−**6**) complexes were assessed utilizing SambVca 2.1 [89]. The generated steric map plot reveals the calculated (% V_{Bur}), corresponding to the steric factor. It is important to note that the steric effect within the catalytic pocket diminishes when transitioning from the red to the blue region in the plot. The steric map was generated by applying the default settings in the SambVca2.1 web tool and incorporating hydrogen atoms. The central reference point for this analysis was gold (Au), with the Au-$C_{carbene}$ bond selected in the z-negative direction. The x-z direction corresponds to the $C_{carbene}$-O bond. We conducted steric map and the percent buried volume (% V_{Bur}) calculations for the (**1**−**6**) compounds, and the results are presented in Supporting Information Table S7. These analyses shed light on the spatial arrangement and steric hindrance within these acetylide complexes, providing valuable insights into their

Table 3
Selected results for the synthesis of amino indolizines by coupling of terminal alkyne, amine and aldehyde catalyzed by the representative catalyst (**1**) and [{(2,6-*t*-Bu_2-C_6H_3O)(NCy_2)}methylidene]AuCl complex.[19,a]

entry	reagent	reagent	reagent	product	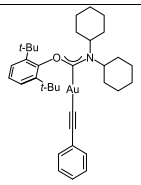 (**1**) yield[b]	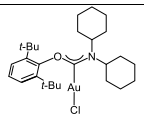 yield[b]
1.				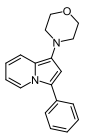 (**19**)	55	47
2.				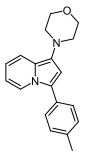 (**20**)	67	61
3.			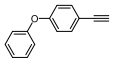	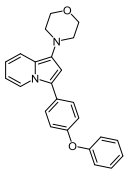 (**21**)	60	69
4.				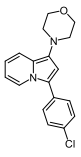 (**22**)	73	52
5.				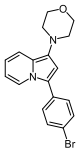 (**23**)	49	41

Reaction conditions: (a). 1:1.2:1.2 ratio of terminal alkynes: morpholine: pyridine-2-carboxyldehyde; 1.00 mol % of catalyst (**1**); 1.00 mol % $AgBF_4$ and 1.00 mol % [{(2,6-*t*-Bu_2-C_6H_3O)(NCy_2)}methylidene]AuCl; 1.00 mol % $AgBF_4$; 2 mL of CH_3CN at 80 °C for the 24 hours. (b). Isolated yields (%).

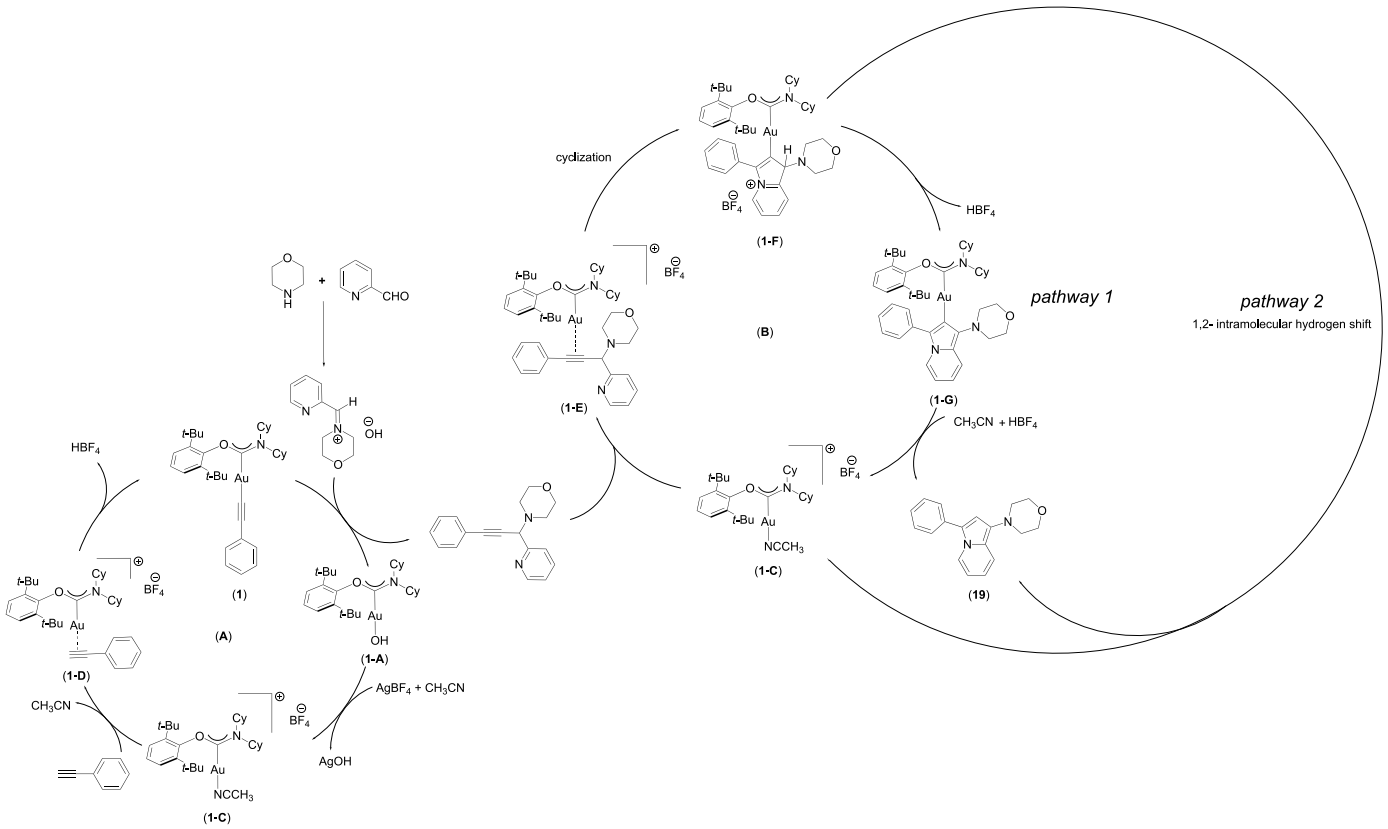

Scheme 3. Proposed mechanism for the Au(I) acyclic aminooxy carbene (AAOC) (**1**) catalyzed the synthesis of amino indolizine by coupling of the representative substrates namely, phenylacetylene, pyridine-2-carboxyldehyde and morpholine.

reactivity and catalytic potential. A comprehensive analysis of the results demonstrated that the (**1**−**3**) complexes, having hydrogen at the *para*-position of the phenoxo ring, exhibit substantial buried volumes (% V_{Bur}) of *ca.* ~72 %. In contrast, the (**4**−**6**) complexes, with the t-butyl group at the para-position of the phenoxy ring, display only marginally higher buried volumes (% V_{Bur}) of 73.2 %, 73.4 %, and 72.8 %, respectively. No significant distinctions were observed between the acyclic aminooxy carbene (AAOC) variants with hydrogen, methyl, and -OPh substitutions at the *para*-position of the gold(I) bound phenyl acetylide moiety.

Catalytic Cycles

The DFT calculations were performed using a simplified gold(I) precatalyst, [{(2,4,6-Me_3-C_6H_2O)(NCy_2)}methylidene]Au[C≡CPh] (**4'**), to reduce the computational cost. The NBO analysis unveils the substantial ionic nature of the Au–C1 [$Au(1)_{(px)19.76\%}$–$C(1)_{(s)80.24\%}$] and Au-C2 [$Au_{(px)16.38\%}$–$C(2)_{(px)83.62\%}$] bonds (Supporting Information Figure S136), displaying over 80% of the electron density donations originating from the respective donor atoms and is attributed to the +1 oxidation state of Au in (**4'**). The Au-C2 bond is slightly more ionic than Au-C1 bond. The optimized structure of (**4'**) reveals several non-covalent Au•••H–C(alkyl) and Au•••H–C(aryl) interactions, with the strongest interaction appearing at 2.671 Å and one Au•••H–C(aryl) interaction appearing at 3.091 Å, in accordance with the range and angles defined for such interactions [50]. NBO analysis indicates moderate donation in *ca.* 2 – 4 kJ/mol from the C−H and C−C σ bond to the Au(*6p*) orbital (See Figure S131). The QTAIM analysis further confirms bond-critical points between the Au(I) and the H atoms (See Fig. 7 and Supporting Information Table S8, Entry 1). The Atoms in molecules (AIM) calculations were performed to investigate the nature of bonding in the molecules between the Au(I) ion and the hydrogens of the ligand system. According to the AIM theory, the closed-shell interactions

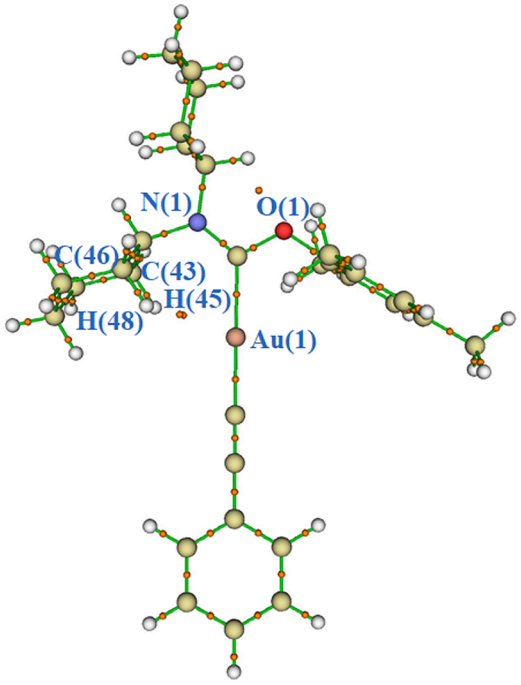

Fig. 7. AIM plot for (4') showing bond critical points (BCP) by red spheres.

include majority of weak intermolecular contacts, that correspond to significantly smaller accumulation of the electron density between the nuclei, so small ρ(r) values and slightly positive $\nabla^2\rho(r)$ values are typical of them [90]. Here Au(1) •••H(45)/H(48) (see Fig. 7 for labelling) found

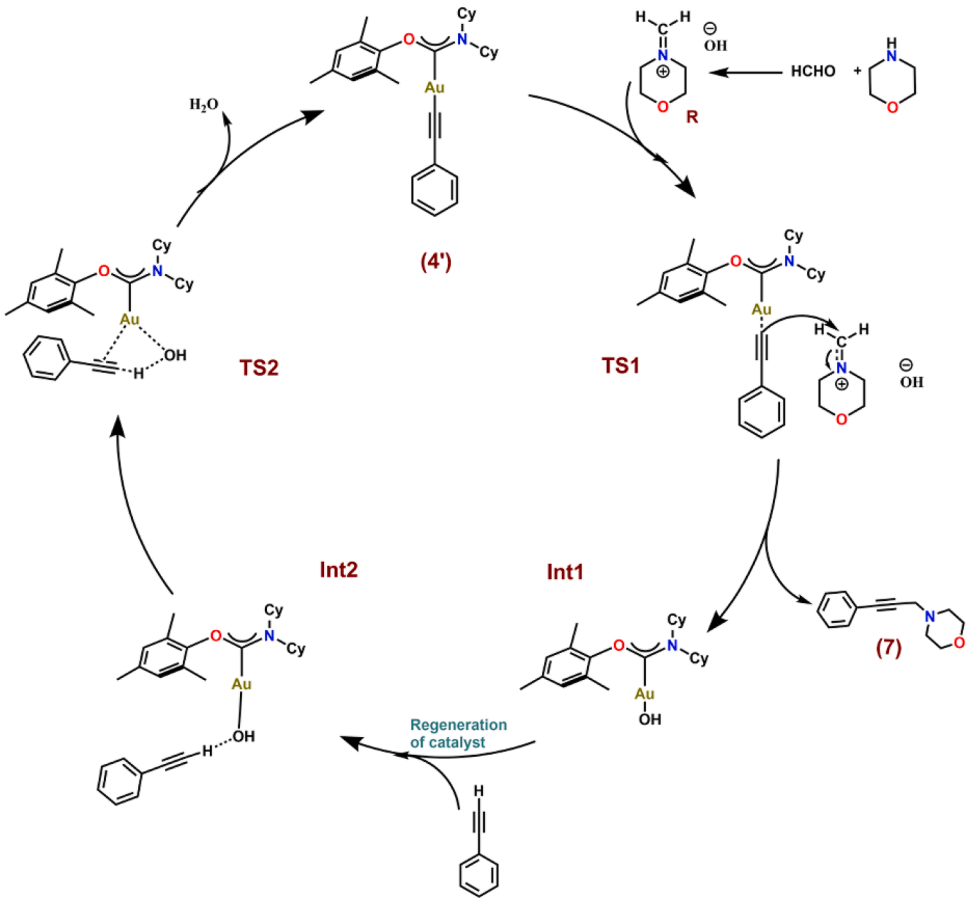

Scheme 4. A proposed mechanism for the A^3 coupling of morpholine, formaldehyde and phenylacetylene substrates forming propargylamine mediated by a gold(I) acetylide (**4'**) complex.

to have the strongest Au•••H−C interaction with decent electron density gradient [$\nabla^2\rho(r)$] values while the Au•••H–C(aryl) interaction is found to have negative $\nabla^2\rho(r)$ value with all five interactions have bond-critical points (BCPs) affirming the presence of non-covalent interactions in (**4'**).

The A^3 coupling reaction

The reaction initiates with the Au(I) bound acetylide moiety in (**4′**) acting as a nucleophile by attacking the carbon atom of the protonated morpholine imine salt, leading to the formation of a C−C bond in the first transition state, **TS1** (Scheme 4). At this transition state, the Au−C2 bond elongates to 2.023 Å from its initial length of 1.988 Å in (**4′**) (Supporting Information Figure S132). Furthermore, there is a slight weakening of the C2≡C3 bond in the acetylide moiety and remarkable bending of ∠ Au1-C2-C3 from 149.8° in **TS1** to 179.7° in (**4′**), and which facilitates the attack of C2 at the carbon atom of imine (C^i) displaying an energy barrier of 36.4 kJ/mol. The attack is accelerated due to the increased negative charge on C2 (Supporting Information Table S9), which helps in migration of the acetylide moiety on the imine salt to form the propargylamine product (**7**) (Supporting Information Figure S133). In the subsequent step, **Int1** is formed after the hydroxide anion in the reaction mixture attaches to the gold(I) (**Int1**) species and the product (**7**). This is evident from the NBO analysis that show the existance of strong covalent bond between C^i and C2 [$C(i)_{(px)49.45\%}$–$C(2)_{(s)50.55\%}$] (Supporting Information Figure S137). The (**Int1**) intermediate is highly exothermic by -144.6 kJ/mol with respect to the reactant.

Subsequently, phenylacetylene enters the coordination sphere of (**Int1**), facilitating the regeneration of catalyst (**4'**) and giving rise to (**Int2**). The hydrogen of phenylacetylene (H^a) is anchored with the oxygen of hydroxide (O2), establishing a weak non-covalent interaction with a distance of 1.948 Å (Supporting Information Figure S134). There is only a slight change in the energy barrier by 0.9 kJ/mol from the preceding species (**Int1**). The interaction of H^a with O2 imparts some ionic character in the C2−H^a bond that can be evident from the NBO analyses, showcasing 64.56% of electron donation from C2 atom and only 35.44% from H^a (Supporting Information Figure S138). In the next step, the formation of (**4'**) occurs *via* (**TS2**), where the π-bond of acetylene attacks the Au(I) and H^a comes closer to the OH^-, having a distance of 1.080 Å and leading to the formation of H_2O Supporting Information Figure S135). In this step, the Au-O2 bond weakens, as seen from a bond distance of 2.256 Å, facilitating the attack of acetylene alongwith the formation of H_2O and ultimately regenerating the catalyst (**4'**). Additionally, the charge on the carbon C2 becomes more negative, signifying the increased nucleophilic nature of C2 as compared to **Int2** (-0.39 *versus* -0.17), (Supporting Information Table S9). The transition state (**TS2**) is associated with an energy barrier of 103.2 kJ/mol relative to the preceding intermediate. However, it is important to note that the overall reaction proceeds along a barrierless pathway. The regenerated catalyst (**4'**), and the propargylamine (**7**), manifests a highly exothermic reaction with an overall energy release of 227.4 kJ/mol (Fig. 8).

To understand the effect of the non-covalent Au•••H–C(alkyl) and Au•••H–C(aryl) interactions during the course of the reaction, we have done AIM analysis for the transition states involved in the catalytic cycle. It has been found that the $\nabla^2\rho(r)_{average}$ of all Au•••H–C(alkyl) and Au•••H–C(aryl) interactions comes as 0.03068 au and 0.03525 au for (**TS1**) and (**TS2**), respectively (See Table S8 entry 2 and 3 for topological diagram and parameters at bond critical point). These values suggest that non-covalent interactions collectively lower the reaction energy barrier. While the role of Au•••H–C non-covalent interactions can not

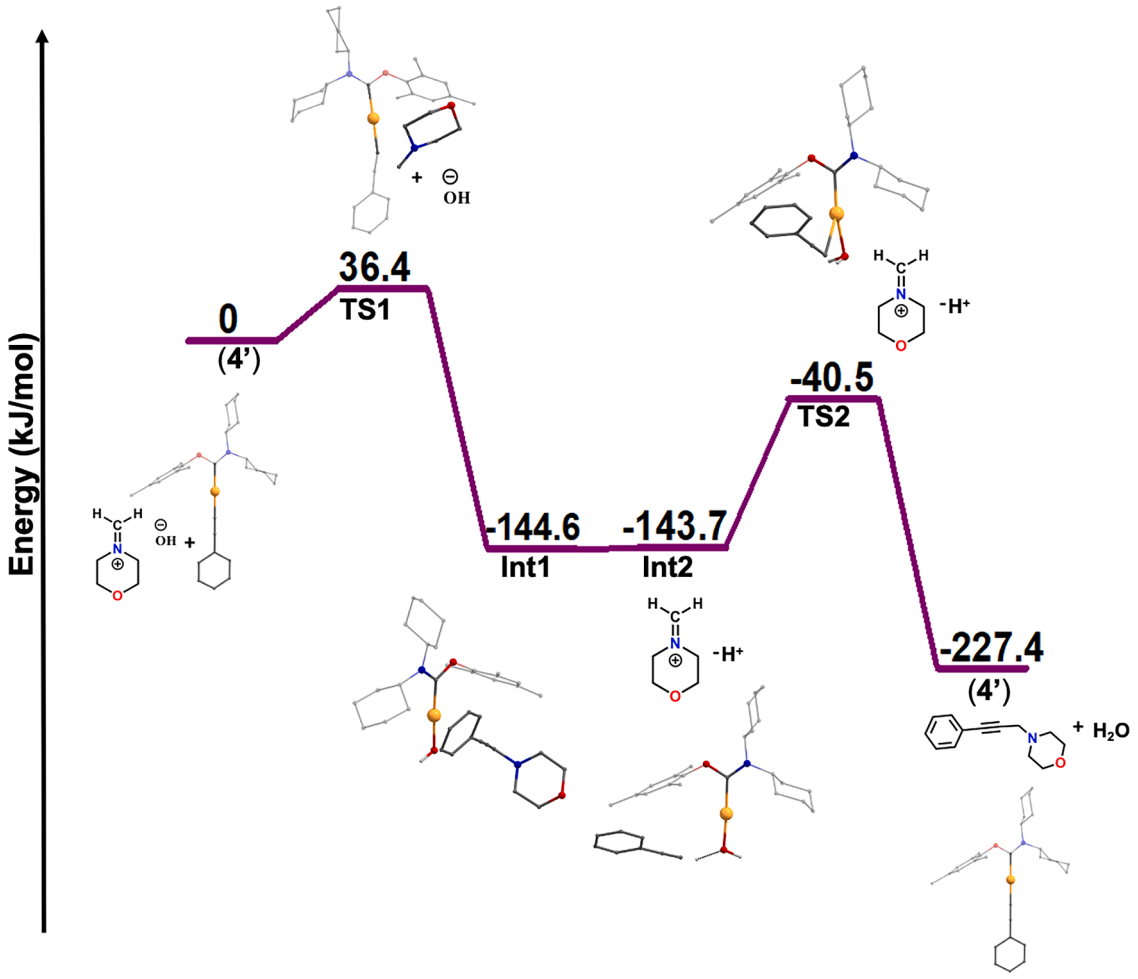

Fig. 8. An energy profile diagram for the A^3 coupling of morpholine, formaldehyde and phenylacetylene substrates forming propargylamine mediated by a gold(I) acetylide (**4'**) complex (Energy in kJ/mol).

be neglected. The absence of the Au•••H–C non-covalent interactions likely contributes to the enhancement of the reaction barrier, suggesting the critical role of these subtle interactions in controlling the overall kinetics of the reaction.

We have also conducted the DFT calculations on another gold(I) precatalyst, the chloro derivative, [{(2,4,6-Me_3-C_6H_2O)(NCy_2)}methylidene]AuCl (**4''**), (Supporting Information Scheme S3 and Figure S139) in addition to the acetylide derivative, [{(2,4,6-Me_3-C_6H_2O)(NCy_2)}methylidene]Au[C≡CPh] (**4'**). In case of (**4''**) (Supporting Information Figure S141), the catalytic cycle initiates with the attack of phenylacetylene at Au(I), resulting in the formation of a Au−C bond. A hydrogen transfer event transpires from the phenylacetylene species to the OH^- resulting in the formation of H_2O and mediated by the intermediates **Int1'** and **Int2'** (Supporting Information Figure S142 and Figure S143). This sequence ultimately gives rise to the (**4'**) species, as shown in Supporting Information Figure S144, which then undergoes regeneration of the reactant species through **TS1'** (Supporting Information Figure S145). The computed natural charges for the cycle is reported in Supporting Information Table S10.

Additionally, the electronic properties of AAOC and NHC ligands were compared by examining their highest occupied molecular orbital (HOMO) and lowest unoccupied molecular orbital (LUMO) orbitals in their gold(I)-acetylide analogues (Figure S156 Supporting Information). The HOMO exhibits similarities between NHC and AAOC ligands, with contributions from the d_{xy} orbital at the Au center. Additionally, in both cases, the LUMO is predominantly located on the carbene carbon center and a minor contribution at the nitrogen and oxygen centers. Also, the HOMO-LUMO gap for NHC (0.1738 au) and AAOC (0.1710 au) gold(I)-acetylide analogues are similar with a difference of 0.0028 au (around 7 kJ/mol).

Tandem A^3 coupling/cyclization reaction

The formation of amino indolizine involves a tandem A^3 coupling/cyclization process in which propargylamine is initially generated in a first catalytic cycle, and undergo subsequent cyclization leading to the desired amino indolizine (**19**) (Scheme 5). The DFT investigations were performed with the same starting gold(I) acetylide species (**4'**). In the first catalytic cycle, shown in red in Fig. 9, the protonated imine derivative formed by the reaction of pyridine-2-carboxaldehyde and morpholine is attacked by the nucleophilic carbon of gold(I) bound phenylacetylide moiety in (**4'**), forming the (**TS^A**) transition state. The observed weakening of the C2≡C3 bond and the alteration of ∠ Au1−C2−C3 from 179.7° in (**4'**) to 136.2° in (**TS^A**) indicate the favorable accessibility for the attack of C2 onto the carbon of the imine (C^i) (Fig. 10a). This C−C bond froming transition state (**TS^A**) has an energy barrier of 64 kJ/mol, as shown in the energy profile in Fig. 9. Subsequently, the intermediate (**A**) (Supporting information Figure S146) forms as the hydroxide anion, present in the reaction mixture, binds to the gold(I) species alongside formation of the propargylamine (**G**). This step has an energy barrier of 23.9 kJ/mol. The binding of OH^- is facilitated by the increased charge of Au (Supporting information Table S11). The reaction proceeds by solvent-mediated intermediate, in which the acetonitrile solvent binds with the Au(I) after the addition of $AgBF_4$ additive, and forming the intermediate (**B**) and AgOH. The

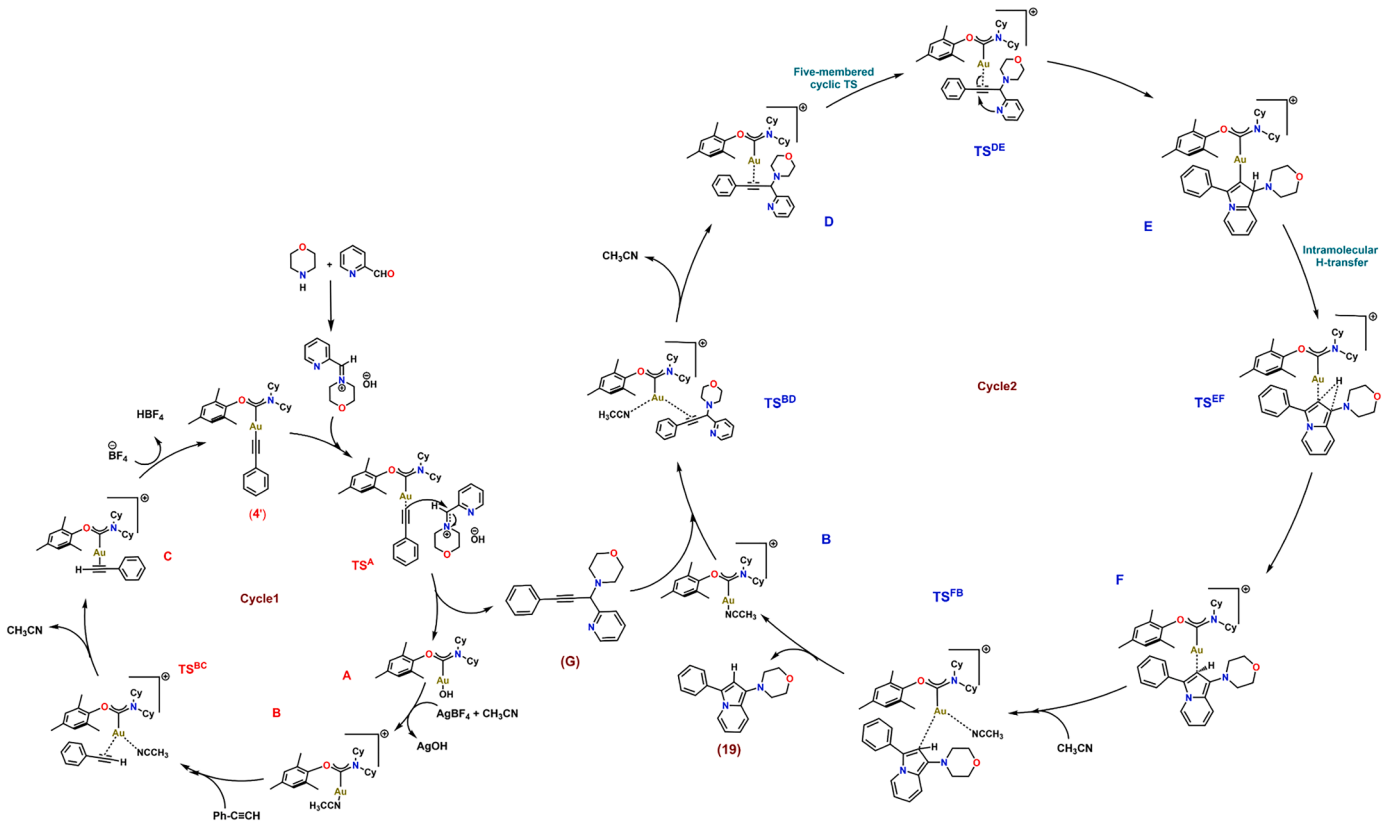

Scheme 5. A proposed tandem A^3 coupling/cyclization of morpholine, pyridine-2-carboxaldehyde and phenylacetylene substrates forming amino indolizine mediated by a gold(I) acetylide (4') complex.

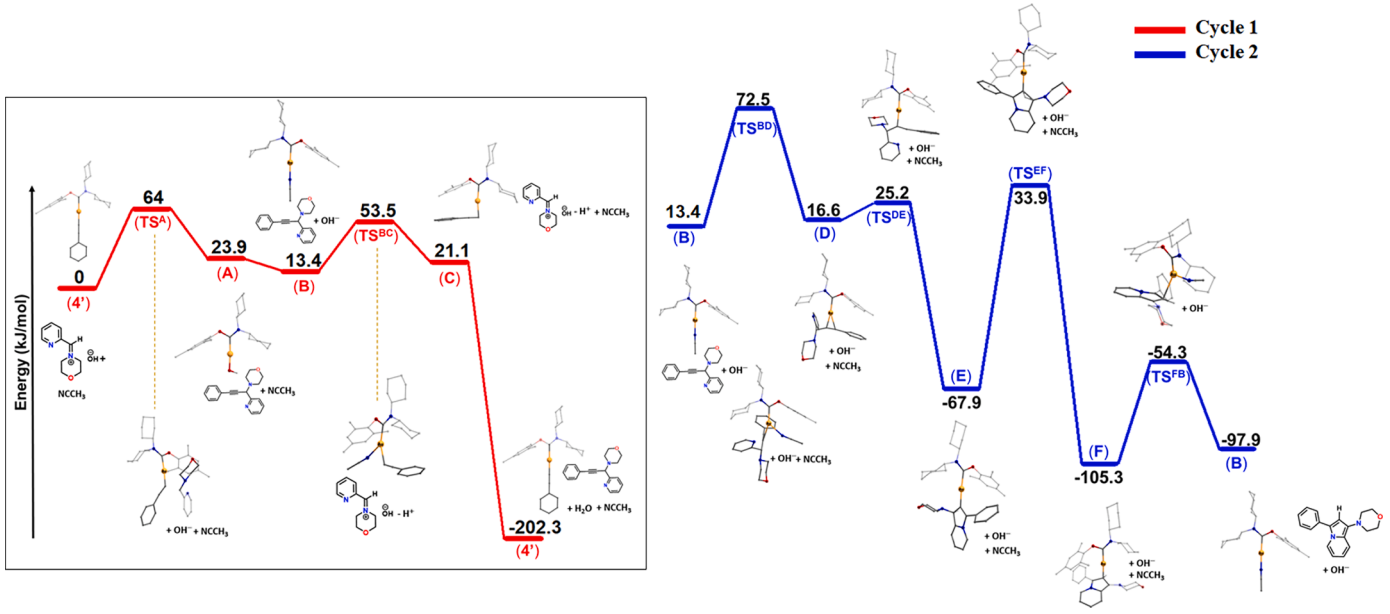

Fig. 9. An energy profile diagram for tandem A^3 coupling/cyclization of morpholine, pyridine-2-carboxaldehyde and phenylacetylene substrates forming amino indolizine mediated by a gold(I) acetylide (4') complex (energy are in kJ/mol).

species (**B**) is formed with the Au1−N2 distance of 2.065 Å (Supporting information Figure S147) and at the expense of 13.4 kJ/mol energy from the starting species (**4'**). The next step proceeds by the incoming phenylacetylene forming (**TS^{BC}**) where C2 starts binding with the Au(I), having the bond distance of Au1-C2 = 2.480 Å and increasing the Au1-N2 distance of 2.424 Å (Supporting information Figure S148). The transition state (**TS^{BC}**) is endothermic by 40.1 kJ/mol with regard to the intermediate (**B**). The intermediate (**C**) involves the formation of a Au−C bond with a bond distance of 2.177 Å (Supporting information Figure S149) displaying an energy barrier of 21.1 kJ/mol. In the next step, BF_4 abstracts the hydrogen attached to C2 of alkyne, forming HBF_4 and consequently regenerating (**4'**) along with the propargylamine (**G**).

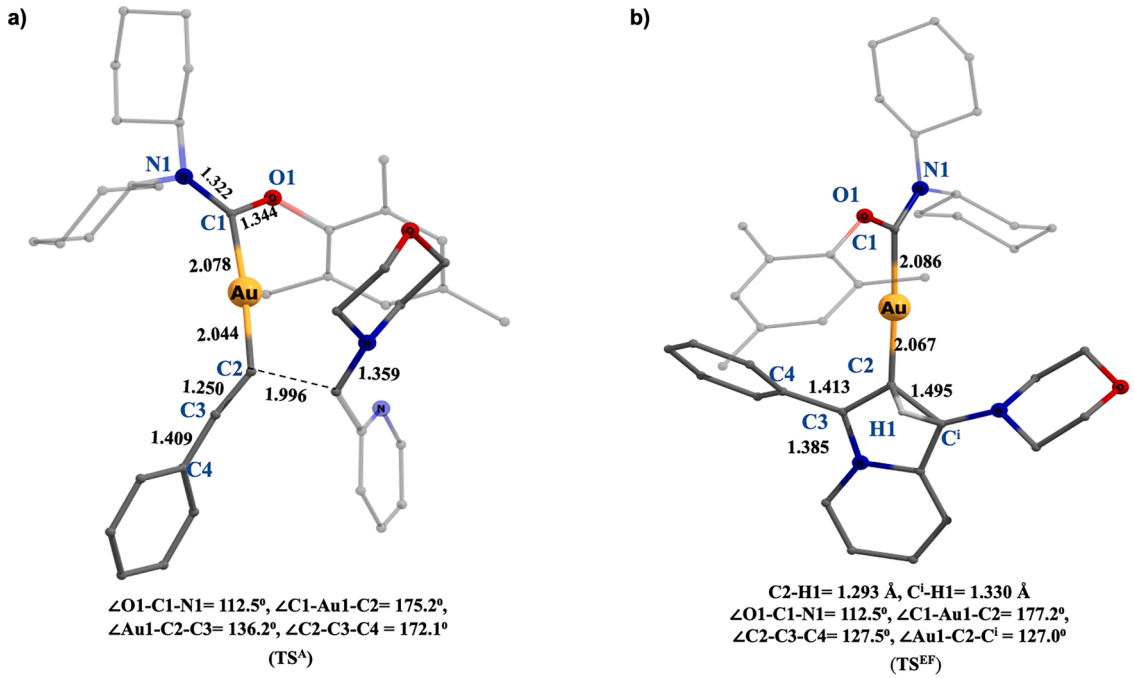

Fig. 10. Optimized geometries of transition states (a) TS^{A} involving the C-C coupling step for the formation of propargylamine (b) TS^{EF} showing the 1,2-intramolecular hydrogen transfer to form amino indolizine (19) product.

This step is highly exothermic by 202.3 kJ/mol compared to the starting species (**4'**).

In the second catalytic cycle, shown in blue in Fig. 9, the propargylamine (**G**) formed in the first cycle reacts with the intermediate (**B**) (Supporting information Figure S147), forming the transition state (**TS^{BD}**) (Supporting information Figure S150) with an energy barrier of 72.5 kJ/mol. The intermediate (**D**) (Supporting information Figure S151) formed in the subsequent step has Au(I) center coordinating to the π-bond of C2−C3 of the propargylamine, and evidenced from the Au−C bond distances of 2.202 Å and 2.366 Å with C2 and C3, respectively. The intermediate (**D**) is stable by 16.6 kJ/mol. The next step is relatively facile leading to the formation of intramolecular five-membered cyclic transition state (**TS^{DE}**) displaying an energy barrier of 25.2 kJ/mol. The formation of the cyclized transition state (**TS^{DE}**) with Au-C2 bond distance of 2.109 Å shows the covalent bond formation between Au1−C2 (Supporting information Figure S152). The cyclized intermediate species (**E**) is stable and exothermic by -67.9 kJ/mol. Notably, there is an observed increase in the charge on nitrogen (N3) to −0.26 when compared to (**TS^{DE}**), which displayed a charge of −0.42 showing the donation of lone pair of N3 to form the cyclic ring (Supporting information Figure S153). The hydrogen attached to C^{i} then undergoes the 1,2-intramolecular hydrogen transfer from C^{i} to C^{2} leading to (**TS^{EF}**). This step has a high energy barrier of 101.8 kJ/mol from (**E**) and an overall energy of 33.9 kJ/mol compared to the starting species (**4'**). This transition state (**TS^{EF}**) formation emphasizes the significance of the intramolecular 1,2-hydrogen transfer step as the rate-determining event in the A^3 coupling reaction for the formation of the amino indolizine (**19**). The C2−H1 distance of 1.293 Å. Subsequently, the intermediate (**F**) is formed with the release of 105.3 kJ/mol energy and in which the amino indolizine so formed is weakly coordinated to the Au(I) center. The Au1-C2 bond in (**F**) (Supporting information Figure S154) elongated by 0.164 Å compared to the previous transition state (**TS^{EF}**) (Fig. 10b). Finally, the acetonitrile solvent molecule coordinates to the gold center forming the transition state (**TS^{FB}**). The energy consumed in this step is 51 kJ/mol, but in overall, it is a barrierless transition state, regenerating the intermediate (**B**) along side the amino indolizine product (**19**). This step is exothermic by 97.9 kJ/mol compared to the starting species (**4'**). The computed natural charges for the cycle is reported in Supporting Information Table S11.

To understand the role of the non-covalent Au•••H–C(alkyl) and Au•••H–C(aryl) interactions in the tandem A^3 coupling/cyclization reaction, the AIM analyses of the important transition states were undertaken, namely of the C−C bond formation in (**TS^{A}**), the intramolecular ring closing in (**TS^{DE}**) and intramolecular hydrogen transfer in (**TS^{EF}**). The order of $\nabla^2\rho(r)_{average}$ is found to be in order **TS^{DE}** (0.04237 au) > **TS^{A}** (0.03380 au) > **TS^{EF}** (0.03288 au), thereby correlating with the energy barriers in reverse trend (Supporting Information Table S12 for topological diagram and parameters at bond critical point). This again suggests the significance of the non-covalent Au•••H–C interactions cannot be neglected.

Conclusion

A series of six new gold(I) acetylide complexes [{(4-R^1-2,6-*t*-Bu_2-C_6H_2O)(NCy_2)}methylidene]Au[C≡C(*p*-$C_6H_4R^2$)] [where R^1 = H; R^2 = H (**1**), Me (**2**), OPh (**3**): R^1 = *t*-Bu; R^2 = H (**4**), Me (**5**), OPh (**6**)] stabilized over acyclic aminooxy carbene (AAOC) ligands have been synthesized and structurally characterized. These (**1**−**6**) complexes successfully catalyzed the A^3-coupling reaction of aldehyde-amine-terminal alkyne to produce propargylamines (**7**−**18**) as well as amino indolizines derivatives (**19**−**23**). Entering the catalytic cycle through its metal-acetylide intermediate using the gold(I) acetylide (**1**) and (**4**) complexes and through its metal-chloro intermediate using the corresponding chloro complexes, [{(2,6-*t*-Bu_2-C_6H_3O)(NCy_2)}methylidene]AuCl and [{(2,4,6-*t*-Bu_3-C_6H_2O)(NCy_2)}methylidene]AuCl, produced near equal product yields, thereby implicating their role in the same catalytic cycle. Significantly enough, a gold(I) bound phenylacetylene intermediate has been detected by mass spectrometric studies. The X-ray photoelectron spectroscopy (XPS) experiments confirmed further corroborated the Au(I) mediated A^3-coupling reactions. The DFT studies showed that for the A^3 coupling reaction, the C-C bond forming step leading to the formation of propargylamine from the gold(I) acetylide (**4'**) complex is endothermic (36.4 kJ/mol) and represents the rate-determing step of the reaction. Notably, amino indolizine product formation utilizes pyridine-based propargylamine, which undergoes cyclization followed by an 1,2-intramolecular hydrogen transfer step.

The hydrogen transfer represents rate-determining step displaying a barrier of 101.8 kJ/mol for the overall tandem A^3 coupling/cyclization reaction. The observed correlation between higher electron density gradients and lower energy barriers emphasizes the pivotal influences of the non-covalent Au•••H–C(alkyl) and Au•••H–C(aryl) interactions. The current study will develop gold(I) acetylide chemistry, particularly their direct use as catalysts in the transition metal-mediated catalytic transformations.

Experimental Section

General Procedures. All manipulations were carried out using standard Schlenk techniques. Solvents were purified and degassed by standard procedures. Phenylacetylene, morpholine, piperidine and benzaldehyde were purchased from Spectrochem Chemicals (India) and 4-ethynyltoluene, 1-ethynyl-4-phenoxybenzene, 1-ethynyl-4-chlorobenzene, and 1-ethynyl-4-bromobenzene were purchased from Sigma Aldrich Chemicals (India) and used without any further purification. ^{1}H NMR, ^{13}C{^{1}H} and ^{19}F{^{1}H} NMR spectra were recorded on Bruker 400 MHz and Bruker 500 MHz NMR spectrometer. ^{1}H NMR peaks are labelled as singlet (s), doublet (d), triplet (t), multiplet (m). The (AAOC) AuCl type complexes was synthesized with the help of procedure reported in the literature [46]. The [1,3-*bis*(2,6-diisopropylphenyl)imidazol-2-ylidene]AuCl and [1,3-*bis*(mesityl)imidazol-2-ylidene]AuCl were synthesized with the help of procedure reported in the literature [62]. The [2,6-*bis*-(1-(*1S*)-menthyl-3-methylene-imidazol-2-ylidene)--pyridine]Au_2Cl_2 was synthesized with the help of procedure reported in the literature [64]. High-resolution mass spectrometry measurements were done on a Micromass Q–Tof spectrometer and a Bruker maxis impact spectrometer. Infrared spectra were recorded on a Perkin Elmer Spectrum One FT-IR spectrometer. Elemental Analysis was carried out on Thermo Quest FLASH 1112 SERIES (CHNS) Elemental Analyser. X-ray photoelectron spectra were acquired on Kartos analytical AXIS Supra spectrometer with a monochromatic Al Kα X-ray source (1486.6 eV) using pass energy of 20 eV. The XPS data was calibrated against C 1s signal peak with binding energy 284.6 eV [91,92] in order to give an accurate binding energy. X-ray diffraction data were collected for compounds (**1**−**6**) on Bruker D8 QUEST single crystal X-ray diffractometer with MoK\a (0.71073) radiation. The Bruker D8 QUEST single crystal X-ray diffractometer was equipped with an Oxford liquid nitrogen cryostream. Crystals were mounted on a nylon loop with paraffin oil. The structures were solved via direct method using SHELXT and refined *via* the full matrix least-squares method with SHELXL-2018/3, refining on F^2 [93]. Crystal data collection and refinement parameters are summarized in Supporting Information Table S1, and CCDC for the gold acetylide complexes, CCDC-2253043 (for **1**), CCDC-2278499 (for **2**), CCDC-2202644 (for **3**), CCDC-2254619 (for **4**), CCDC-2186065 (for **5**), CCDC-2192674 (for **6**) CCDC-2278453 (for **20**), and CCDC-2281829 (for **23**) contain the supplementary crystallographic data for this paper. These data can be obtained free of charge from the Cambridge Crystallographic Data centre *via* www.ccdc.cam.ac.uk/data_request/cif.

Synthesis of [{(2,6-t-Bu$_2$-C$_6$H$_3$O)(NCy$_2$)}methylidene]Au(C≡CC$_6$H$_5$) (1)

A mixture of [{(2,6-*t*-Bu_2-C_6H_3O)(NCy_2)}methylidene]AuCl (0.030 g, 0.047 mmol) was taken with the phenylacetylene (0.024 g, 0.235 mmol) and K_2CO_3 (0.065 g, 0.470 mmol) added to it in dry CH_2Cl_2 (*ca.* 10 mL). The reaction mixture was stirred at room temperature for 24 hours. Afterward, the volatiles were removed in *vacuo*, and the residue was dissolved in CH_2Cl_2 (*ca.* 50 mL), and filtered through the thin layer of neutral alumina. Then the solvent was evaporated and obtained residue was washed with the pentane and dried under vacuum to give the product (**1**) as a white solid (0.029 g, 88 %). ^{1}H NMR ($CDCl_3$, 400 MH_Z, 25 °C): δ ppm, 7.38−7.35 (m, 4H, *m*-$C_6\underline{H}_3$ and *o*-$C_6\underline{H}_5$), 7.22 (t, 1H, $^3J_{HH}$ = 8 Hz, *p*-$C_6\underline{H}_3$), 7.16 (t, 2H, $^3J_{HH}$ = 7 Hz, *m*-$C_6\underline{H}_5$), 7.09 (t, 1H, $^3J_{HH}$ = 7 Hz, *p*-$C_6\underline{H}_5$), 4.96−4.91 (m, 1H, $NC_6\underline{H}_{11}$), 3.27 (br, 1H, $NC_6\underline{H}_{11}$), 1.96−1.75 (m, 12H, $2C_6\underline{H}_{11}$), 1.65−1.44 (m, 8H, $2C_6\underline{H}_{11}$), 1.41 (s, 18H, $2C(C\underline{H}_3)_3$). ^{13}C{^{1}H} NMR ($CDCl_3$, 100 MHz, 25 °C): δ ppm, 227.6 (Au−$\underline{C}_{carbene}$), 155.0 (*ipso*-$\underline{C}_6H_3$), 141.9 (*o*-$\underline{C}_6H_3$), 132.4 (*o*-$\underline{C}_6H_5$), 127.5 (*m*-$\underline{C}_6H_3$), 126.9 (*m*-$\underline{C}_6H_5$), 126.1 (*ipso*-$\underline{C}_6H_5$), 126.0 (*p*-$\underline{C}_6H_3$), 125.8 (*p*-$\underline{C}_6H_5$), 124.2 ($\underline{C}$≡$\underline{C}C_6H_5$), 105.2 (C≡$\underline{C}C_6H_5$), 59.4 ($N\underline{C}_6H_{11}$), 57.6 ($N\underline{C}_6H_{11}$), 35.4 ($2\underline{C}(CH_3)_3$), 34.7 ($\underline{C}_6H_{11}$), 32.3 ($2C(\underline{C}H_3)_3$), 29.8 ($\underline{C}_6H_{11}$) 26.7 ($\underline{C}_6H_{11}$), 25.4 ($\underline{C}_6H_{11}$), 25.1 ($\underline{C}_6H_{11}$), 24.8 ($\underline{C}_6H_{11}$). IR data (cm^{-1}) KBr pellet: 3967 (w), 3453 (m), 3075 (w), 2930 (s), 2854 (s), 2107 (w), 1596 (w), 1517 (s), 1486 (m), 1448 (m), 1415 (m), 1375 (w), 1317 (m), 1210 (s), 1142 (m), 1118 (w), 1029 (m), 897 (w), 783 (w), 758 (s), 696 (w). HRMS (ESI): calcd. for $[C_{35}H_{48}AuNO + H]^+$ *m/z* 696.3474; found *m/z* 696.3476. Anal. Calcd. for $C_{35}H_{48}AuNO$: C, 60.42; H, 6.95; N, 2.01; found: C, 60.06; H, 7.07; N, 1.26 %.

Synthesis of [{(2,6-t-Bu$_2$-C$_6$H$_3$O)(NCy$_2$)}methylidene]Au[C≡C(p-C$_6$H$_4$CH$_3$)] (2)

A mixture of [{(2,6-*t*-Bu_2-C_6H_3O)(NCy_2)}methylidene]AuCl (0.060 g, 0.095 mmol) was taken with the 4-ethynyltoluene (0.055 g, 0.475 mmol) and K_2CO_3 (0.131 g, 0.950 mmol) added to it in dry CH_2Cl_2 (*ca.* 20 mL). The reaction mixture was stirred at room temperature for 24 hours. Afterward, the volatiles were removed in *vacuo*, and the residue was dissolved in CH_2Cl_2 (*ca.* 50 mL), and filtered through the thin layer of neutral alumina. Then the solvent was evaporated and obtained residue was washed with the pentane and dried under vacuum to give the product (**2**) as a white solid (0.062 g, 92 %). ^{1}H NMR ($CDCl_3$, 400 MH_Z, 25 °C): δ ppm, 7.36 (d, 2H, $^3J_{HH}$ = 8 Hz, *m*-$C_6\underline{H}_3$), 7.26 (d, 2H, $^3J_{HH}$ = 8 Hz, *o*-$C_6\underline{H}_4CH_3$), 7.22 (t, 1H, $^3J_{HH}$ = 7 Hz, *p*-$C_6\underline{H}_3$), 6.96 (d, 2H, $^3J_{HH}$ = 8 Hz, *m*-$C_6\underline{H}_4CH_3$), 4.96−4.90 (m, 1H, $NC_6\underline{H}_{11}$), 3.28 (br, 1H, $NC_6\underline{H}_{11}$), 2.28 (s, 3H, $C_6H_4C\underline{H}_3$), 1.96−1.75 (m, 10H, $2C_6\underline{H}_{11}$), 1.64−1.43 (m, 6H, $2C_6\underline{H}_{11}$), 1.41 (s, 18H, $2C(C\underline{H}_3)_3$), 1.28−1.21 (m, 4H, $2C_6\underline{H}_{11}$). ^{13}C{^{1}H} NMR ($CDCl_3$, 100 MHz, 25 °C): δ ppm, 227.6 (Au−$\underline{C}_{carbene}$), 155.0 (*ipso*-$\underline{C}_6H_3$), 141.9 (*o*-$\underline{C}_6H_3$), 135.5 (*ipso*-$\underline{C}_6H_4CH_3$), 132.2 (*m*-$\underline{C}_6H_3$), 128.3 (*p*-$\underline{C}_6H_3$), 126.9 (*o*-$\underline{C}_6H_4CH_3$), 125.9 (*m*-$\underline{C}_6H_4CH_3$), 123.0 (*p*-$\underline{C}_6H_4CH_3$), 122.9 ($\underline{C}$≡$\underline{C}C_6H_4CH_3$), 105.2 (C≡$\underline{C}C_6H_4CH_3$), 59.3 ($N\underline{C}_6H_{11}$), 57.5 ($N\underline{C}_6H_{11}$), 35.4 ($2\underline{C}(CH_3)_3$), 34.7 ($\underline{C}_6H_{11}$), 32.3 ($2C(\underline{C}H_3)_3$), 29.8 ($\underline{C}_6H_{11}$) 26.7 ($\underline{C}_6H_{11}$), 25.4 ($\underline{C}_6H_{11}$), 25.1 ($\underline{C}_6H_{11}$), 24.8 ($\underline{C}_6H_{11}$), 21.3 ($C_6H_4\underline{C}H_3$). IR data (cm^{-1}) KBr pellet: 3479 (w), 2927 (s), 2853 (s), 2116 (w), 1740 (m), 1507 (s), 1448 (m), 1415 (m), 1368 (m), 1311 (m), 1269 (w), 1213 (s), 1142 (w), 1118 (w), 1029 (m), 894 (w), 812 (w). HRMS (ESI): calcd. for $[C_{36}H_{50}AuNO + H]^+$ *m/z* 710.3631; found *m/z* 710.3633. Anal. Calcd. for $C_{36}H_{50}AuNO$: C, 60.92; H, 7.10; N, 1.97; Found: C, 60.32; H, 7.07; N, 1.51 %.

Synthesis of [{(2,6-t-Bu$_2$-C$_6$H$_3$O)(NCy$_2$)}methylidene]Au[C≡C(p-C$_6$H$_4$OC$_6$H$_5$)] (3)

A mixture of [{(2,6-*t*-Bu_2-C_6H_3O)(NCy_2)}methylidene]AuCl (0.040 g, 0.063 mmol) was taken with the 1-ethynyl-4-phenoxybenzene (0.061 g, 0.315 mmol) and K_2CO_3 (0.087 g, 0.630 mmol) added to it in dry CH_2Cl_2 (*ca.* 15 mL). The reaction mixture was stirred at room temperature for 24 hours. Afterward, the volatiles were removed in *vacuo*, and the residue was dissolved in CH_2Cl_2 (*ca.* 50 mL), and filtered through the thin layer of neutral alumina. Then the solvent was evaporated and obtained residue was washed with the pentane and dried under vacuum to give the product (**3**) as a white solid (0.047 g, 95 %). ^{1}H NMR ($CDCl_3$, 400 MH_Z, 25 °C): δ ppm, 7.38−7.29 (m, 6H, *m*-$C_6\underline{H}_3$ and $C_6\underline{H}_4OC_6\underline{H}_5$), 7.22 (t, 1H, $^3J_{HH}$ = 8 Hz, *p*-$C_6\underline{H}_3$), 7.07 (t, 1H, $^3J_{HH}$ = 7 Hz, *p*-$OC_6\underline{H}_5$), 6.96 (d, 2H, $^3J_{HH}$ = 8 Hz, *o*-$OC_6\underline{H}_5$), 6.82 (d, 2H, $^3J_{HH}$ = 8 Hz *m*-$C_6\underline{H}_4$), 4.96−4.91 (m, 1H, $NC_6\underline{H}_{11}$), 3.27 (br, 1H, $NC_6\underline{H}_{11}$), 1.96−1.75 (m, 10H, $C_6\underline{H}_{11}$), 1.65−1.45 (m, 6H, $C_6\underline{H}_{11}$), 1.41 (s, 18H, $2C(C\underline{H}_3)_3$), 1.36−1.22 (m, 4H, $C_6\underline{H}_{11}$). ^{13}C{^{1}H} NMR ($CDCl_3$, 100 MHz, 25 °C): δ ppm, 227.5 (Au−$\underline{C}_{carbene}$), 157.4 (*ipso*-$\underline{C}_6H_5$), 155.1 (*p*-$\underline{C}_6H_4$), 155.0 (*ipso*-$\underline{C}_6H_3$), 141.9 (*o*-$\underline{C}_6H_3$), 133.8 (*o*-$\underline{C}_6H_4$), 129.6 (*m*-$\underline{C}_6H_5$), 126.9 (*m*-$\underline{C}_6H_3$), 126.0 (*p*-$\underline{C}_6H_3$), 123.4 ($\underline{C}$≡$\underline{C}C_6H_4$) 122.9 (*p*-$\underline{C}_6H_5$), 121.4 (*ipso*-C_6H_4), 118.6 (*o*-

$\underline{C}_6H_5$) 118.4 (*m*-$\underline{C}_6H_4$), 104.5 (C≡$\underline{C}C_6H_4$), 59.4 (N$\underline{C}_6H_{11}$), 57.6 (N$\underline{C}_6H_{11}$), 35.4 (2$\underline{C}(CH_3)_3$), 34.7 ($\underline{C}_6H_{11}$), 32.3 (2C($\underline{C}H_3)_3$), 29.8 ($\underline{C}_6H_{11}$), 26.7 ($\underline{C}_6H_{11}$), 25.4 ($\underline{C}_6H_{11}$), 25.1 ($\underline{C}_6H_{11}$), 24.8 ($\underline{C}_6H_{11}$). IR data (cm^{-1}) KBr pellet: 2924 (s), 2855 (m), 2113 (w), 1586 (s) 1518 (s), 1497 (s), 1487 (s), 1445 (s), 1416 (m), 1368 (m), 1312 (m), 1269 (s), 1238 (s), 1213 (s), 1143 (w), 1118 (w), 1019 (m), 870 (w), 828 (m), 796 (w), 779 (w), 753 (w), 694 (w), 528 (w), 478 (w). HRMS (ESI): calcd. for $[C_{41}H_{52}AuNO_2 + H]^+$ *m/z* 788.3737; found *m/z* 788.3726. Anal. Calcd. for $C_{41}H_{52}AuNO_2$: C, 62.51; H, 6.65; N, 1.78; found: C, 62.09; H, 6.91; N, 1.54 %.

Synthesis of [{(2,4,6-t-Bu$_3$-C$_6$H$_2$O)(NCy$_2$)}methylidene]Au(C≡CC$_6$H$_5$) (4)

A mixture of [{(2,4,6-*t*-Bu$_3$-C$_6$H$_2$O)(NCy$_2$)}methylidene]AuCl (0.050 g, 0.072 mmol) was taken with the phenylacetylene (0.037 g, 0.360 mmol) and K_2CO_3 (0.099 g, 0.720 mmol) added to it in dry CH_2Cl_2 (*ca.* 15 mL). The reaction mixture was stirred at room temperature for 24 hours. Afterward, the volatiles were removed in *vacuo*, and the residue was dissolved in CH_2Cl_2 (*ca.* 50 mL), and filtered through the thin layer of neutral alumina. Then the solvent was evaporated and obtained residue was washed with the pentane and dried under vacuum to give the product (**4**) as a white solid (0.050 g, 93 %). ^{1}H NMR ($CDCl_3$, 400 MH$_Z$, 25 °C): δ ppm, 7.37 (s, 2H, C$_6\underline{H}_2$), 7.31 (d, 2H, $^3J_{HH}$ = 7 Hz, *o*-C$_6\underline{H}_5$), 7.15 (t, 2H, $^3J_{HH}$ = 7 Hz, *m*-C$_6\underline{H}_5$), 7.08 (t, 1H, $^3J_{HH}$ = 7 Hz, *p*-C$_6\underline{H}_5$), 4.92 (br, 1H, NC$_6\underline{H}_{11}$), 3.23 (br, 1H, NC$_6\underline{H}_{11}$), 1.95−1.75 (m, 12H, 2C$_6\underline{H}_{11}$), 1.64−1.52 (m, 8H, 2C$_6\underline{H}_{11}$), 1.41 (s, 18H, 2C(C$\underline{H}_3)_3$), 1.38 (s, 9H, C(C$\underline{H}_3)_3$). ^{13}C{^{1}H} NMR ($CDCl_3$, 100 MHz, 25 °C): δ ppm, 227.9 (Au−$\underline{C}_{carbene}$), 153.0 (*ipso*-$\underline{C}_6H_2$), 147.9 (*p*-$\underline{C}_6H_2$), 140.8 (*o*-$\underline{C}_6H_2$), 132.2 (*o*-$\underline{C}_6H_5$), 127.5 (*m*-$\underline{C}_6H_5$), 126.3 (*ipso*-$\underline{C}_6H_5$), 125.6 (*p*-$\underline{C}_6H_5$), 123.9 ($\underline{C}$≡CC_6H_5), 123.7 (*m*-$\underline{C}_6H_2$), 104.8 (C≡$\underline{C}C_6H_5$), 59.3 (N$\underline{C}_6H_{11}$), 57.5 (N$\underline{C}_6H_{11}$), 35.5 (2$\underline{C}(CH_3)_3$), 34.9 ($\underline{C}_6H_{11}$), 34.7 ($\underline{C}_6H_{11}$), 32.3 (2C($\underline{C}H_3)_3$) 31.5 (C($\underline{C}H_3)_3$), 29.8 ($\underline{C}_6H_{11}$), 26.7 ($\underline{C}(CH_3)_3$), 25.4 ($\underline{C}_6H_{11}$), 25.2 ($\underline{C}_6H_{11}$), 24.8 ($\underline{C}_6H_{11}$). IR data (cm^{-1}) KBr pellet: 3445 (br), 3073 (w), 2960 (s), 2936 (s), 2857 (m), 2117 (w), 1596 (m), 1526 (s), 1484 (w), 1450 (w), 1430 (w), 1393 (w), 1362 (m), 1313 (w), 1271 (w), 1247 (w), 1201 (s), 1133 (m), 1115 (m), 1032 (m), 896 (w), 831 (w), 786 (w), 754 (s), 690 (w), 621 (w), 526 (w). HRMS (ESI): calcd. for $[C_{39}H_{56}AuNO + H]^+$ *m/z* 752.4100; found *m/z* 752.4096. Anal. Calcd. for $C_{39}H_{56}AuNO$: C, 62.30; H, 7.51; N, 1.86; found: C, 61.80; H, 7.53; N, 1.56 %.

Synthesis of [{(2,4,6-t-Bu$_3$-C$_6$H$_2$O)(NCy$_2$)}methylidene]Au[C≡C(p-C$_6$H$_4$CH$_3$)] (5)

A mixture of [{(2,4,6-*t*-Bu$_3$-C$_6$H$_2$O)(NCy$_2$)}methylidene]AuCl (0.050 g, 0.072 mmol) was taken with the 4-ethynyltoluene (0.042 g, 0.360 mmol) and K_2CO_3 (0.099 g, 0.720 mmol) added to it in dry CH_2Cl_2 (*ca.* 15 mL). The reaction mixture was stirred at room temperature for 24 hours. Afterward, the volatiles were removed in *vacuo*, and the residue was dissolved in CH_2Cl_2 (*ca.* 50 mL), and filtered through the thin layer of neutral alumina. Then the solvent was evaporated and obtained residue was washed with the pentane and dried under vacuum to give the product (**5**) as a white solid (0.051 g, 93 %). ^{1}H NMR ($CDCl_3$, 400 MH$_Z$, 25 °C): δ ppm, 7.37 (s, 2H, C$_6\underline{H}_2$), 7.21 (d, 2H, $^3J_{HH}$ = 8 Hz, C$_6\underline{H}_4$CH$_3$), 6.96 (d, 2H, $^3J_{HH}$ = 8 Hz, C$_6\underline{H}_4$CH$_3$), 4.92 (br, 1H, NC$_6\underline{H}_{11}$), 3.23 (br, 1H, NC$_6\underline{H}_{11}$), 2.28 (s, 3H, C$_6$H$_4$C$\underline{H}_3$), 1.94−1.83 (m, 10H, 2C$_6\underline{H}_{11}$), 1.77−1.54 (m, 10H, 2C$_6\underline{H}_{11}$), 1.40 (s, 18H, 2C(C$\underline{H}_3)_3$), 1.38 (s, 9H, C(C$\underline{H}_3)_3$). ^{13}C{^{1}H} NMR ($CDCl_3$, 100 MHz, 25 °C): δ ppm, 227.8 (Au−$\underline{C}_{carbene}$), 153.0 (*ipso*-$\underline{C}_6H_2$), 147.9 (*p*-$\underline{C}_6H_2$), 140.8 (*o*-$\underline{C}_6H_2$), 135.3 (*p*-$\underline{C}_6H_4$), 132.1 (*o*-$\underline{C}_6H_4$), 128.3 (*m*-$\underline{C}_6H_4$), 123.6 (*m*-$\underline{C}_6H_2$), 123.2 ($\underline{C}$≡CC_6H_4), 123.0 (*ipso*-$\underline{C}_6H_4$), 104.9 (C≡$\underline{C}C_6H_4$), 59.3 (N$\underline{C}_6H_{11}$), 57.4 (N$\underline{C}_6H_{11}$), 35.5 (2$\underline{C}(CH_3)_3$), 34.9 ($\underline{C}_6H_{11}$), 34.7 ($\underline{C}_6H_{11}$), 32.3 (2C($\underline{C}H_3)_3$) 31.5 (C($\underline{C}H_3)_3$), 29.8 ($\underline{C}_6H_{11}$), 26.7 ($\underline{C}(CH_3)_3$), 25.4 ($\underline{C}_6H_{11}$), 25.2 ($\underline{C}_6H_{11}$), 24.8 ($\underline{C}_6H_{11}$), 21.3 ($\underline{C}H_3$). IR data (cm^{-1}) KBr pellet: 3435 (br), 2933 (s), 2859 (m), 2118 (w), 1672 (w), 1594 (w), 1519 (m), 1447 (m), 1362 (w), 1314 (w), 1207 (s), 1119 (m), 1029 (m), 879 (w), 815 (w), 622 (w), 527 (w). HRMS (ESI): calcd. for $[C_{40}H_{58}AuNO + K]^+$ *m/z* 804.3816;found *m/z* 804.3820. Anal. Calcd. for $C_{40}H_{58}AuNO$: C, 62.73; H, 7.63; N, 1.83; found: C, 61.95; H, 7.25; N, 1.65 %.

Synthesis of [{(2,4,6-t-Bu$_3$-C$_6$H$_2$O)(NCy$_2$)}methylidene]Au[C≡C(p-C$_6$H$_4$OC$_6$H$_5$)] (6)

A mixture of [{(2,4,6-*t*-Bu$_3$-C$_6$H$_2$O)(NCy$_2$)}methylidene]AuCl (0.035 g, 0.051 mmol) was taken with the 1-ethynyl-4-phenoxybenzene (0.049 g, 0.255 mmol) and K_2CO_3 (0.070 g, 0.510 mmol) added to it in dry CH_2Cl_2 (*ca.* 15 mL). The reaction mixture was stirred at room temperature for 24 hours. Afterward, the volatiles were removed in *vacuo*, and the residue was dissolved in CH_2Cl_2 (*ca.* 50 mL), and filtered through the thin layer of neutral alumina. Then the solvent was evaporated and obtained residue was washed with the pentane and dried under vacuum to give the product (**6**) as a white solid (0.039 g, 91 %). ^{1}H NMR ($CDCl_3$, 400 MH$_Z$, 25 °C): δ ppm, 7.37 (s, 2H, C$_6\underline{H}_2$), 7.31 (t, 2H, *m*-OC$_6\underline{H}_5$), 7.28 (d, 2H, $^3J_{HH}$ = 8 Hz, *o*-C$_6\underline{H}_4$), 7.07 (t, 1H, $^3J_{HH}$ = 8 Hz, *p*-OC$_6\underline{H}_5$), 6.96 (d, 2H, $^3J_{HH}$ = 8 Hz, *o*-OC$_6\underline{H}_5$), 6.81 (d, 2H, $^3J_{HH}$ = 8 Hz, *m*-C$_6\underline{H}_4$), 4.92−4.89 (m, 1H, NC$_6\underline{H}_{11}$), 3.23 (br, 1H, NC$_6\underline{H}_{11}$), 1.95−1.75 (m, 14H, C$_6\underline{H}_{11}$), 1.67−1.54 (m, 6H, C$_6\underline{H}_{11}$), 1.41 (s, 18H, 2C(C$\underline{H}_3)_3$), 1.39 (s, 9H, C(C$\underline{H}_3)_3$). ^{13}C{^{1}H} NMR ($CDCl_3$, 100 MHz, 25 °C): δ ppm, 227.8 (Au−$\underline{C}_{carbene}$), 157.5 (*ipso*-$\underline{C}_6H_5$), 155.0 (*p*-$\underline{C}_6H_4$), 153.0 (*ipso*-$\underline{C}_6H_2$), 147.9 (*p*-$\underline{C}_6H_2$), 140.8 (*o*-$\underline{C}_6H_2$), 133.6 (*o*-$\underline{C}_6H_4$), 129.6 (*m*-$\underline{C}_6H_5$), 123.6 (*m*-$\underline{C}_6H_2$), 123.5 ($\underline{C}$≡CC_6H_4), 122.9 (*p*-$\underline{C}_6H_5$), 121.6 (*ipso*-C_6H_4), 118.6 (*o*-$\underline{C}_6H_5$), 118.3 (*m*-$\underline{C}_6H_4$), 104.1 (C≡$\underline{C}C_6H_4$), 59.3 (N$\underline{C}_6H_{11}$), 57.5 (N$\underline{C}_6H_{11}$), 35.5 (2$\underline{C}(CH_3)_3$), 34.9 ($\underline{C}_6H_{11}$), 34.7 ($\underline{C}_6H_{11}$), 32.3 (2C($\underline{C}H_3)_3$), 31.5 (C($\underline{C}H_3)_3$), 29.8 ($\underline{C}_6H_{11}$), 26.7 ($\underline{C}(CH_3)_3$) 25.4 ($\underline{C}_6H_{11}$), 25.2 ($\underline{C}_6H_{11}$), 24.8 ($\underline{C}_6H_{11}$). IR data (cm^{-1}) KBr pellet: 3433 (br), 2936 (s), 2858 (s), 2202 (w), 2119 (w), 1587 (m), 1519 (s), 1486 (s), 1361 (w), 1313 (w), 1235 (s), 1206 (s), 1116 (m), 1016 (m), 866 (w), 831 (w), 780 (w), 692 (w). HRMS (ESI): calcd. for $[C_{45}H_{60}AuNO_2 + H]^+$ *m/z* 844.4363;found *m/z* 844.4365. Anal. Calcd. for $C_{45}H_{60}AuNO_2$: C, 64.04; H, 7.17; N, 1.66; found: C, 63.22; H, 6.84; N, 1.47 %.

General procedure for the blank experiment

In typical catalysis run, a mixture of the phenylacetylene (1.00 mmol) was taken CH_3CN (*ca.* 2 mL) in reaction vial and kept at 80 °C and after 5 minutes formaldehyde (4.00 mmol) and morpholine (1.20 mmol) was added to it. Reaction mixture was stirred for the 24 hours at 80 °C. Afterward, it was cooled to room temperature and volatiles were evaporated and obtained residue was purified by column chromatography using neutral alumina as the stationary phase and mixed medium of petroleum ether and EtOAc as mobile phase to give the pure product (**7**) that was confirmed by ^{1}H NMR, GCMS and elemental analysis (Entry 1 in Supporting Information Table S5 and Figures S49−S52).

General procedure for the control experiment

The following control experiments were performed.

(*i*). In typical catalysis run, a mixture of the phenylacetylene (1.00 mmol) was taken with ligand {[(2,6-*t*-Bu$_2$-C$_6$H$_3$O)(NCy$_2$)]CH}$^+$OTf$^-$ (0.005 mmol, 0.5 mol %) in CH_3CN (*ca.* 2 mL) in reaction vial and kept at 80 °C and after 5 minutes formaldehyde (4.00 mmol) and morpholine (1.20 mmol) was added to it. Reaction mixture was stirred for the 24 hours at 80 °C. Afterward, it was cooled to room temperature and volatiles were evaporated and obtained residue was purified by column chromatography using neutral alumina as the stationary phase and mixed medium of petroleum ether and EtOAc as mobile phase to give the pure product (**7**) that was confirmed by ^{1}H NMR, GCMS and elemental analysis (Entry 2 in Supporting Information Table S5 and Figures S49−S52).

(*ii*). In typical catalysis run, a mixture of the phenylacetylene (1.00 mmol) was taken with (Me_2S)AuCl (0.005 mmol, 0.5 mol %) in CH_3CN (*ca.* 2 mL) in reaction vial and kept at 80 °C and after 5 minutes

formaldehyde (4.00 mmol) and morpholine (1.20 mmol) was added to it. Reaction mixture was stirred for the 24 hours at 80 °C. Afterward, it was cooled to room temperature and volatiles were evaporated and obtained residue was purified by column chromatography using neutral alumina as the stationary phase and mixed medium of petroleum ether and EtOAc as mobile phase to give the pure product (**7**) that was confirmed by ^{1}H NMR, GCMS and elemental analysis (Entry 3 in Supporting Information Table S5 and Figures S49−S52).

(*iii*). In typical catalysis run, a mixture of the phenylacetylene (1.00 mmol) was taken with [{(2,6-*t*-Bu$_2$-C$_6$H$_3$O)(NCy$_2$)}methylidene]AuCl (0.005 mmol, 0.5 mol %) in CH$_3$CN (*ca.* 2 mL) in reaction vial and kept at 80 °C and after 5 minutes formaldehyde (4.00 mmol) and morpholine (1.20 mmol) was added to it. Reaction mixture was stirred for the 24 hours at 80 °C. Afterward, it was cooled to room temperature and volatiles were evaporated and obtained residue was purified by column chromatography using neutral alumina as the stationary phase and mixed medium of petroleum ether and EtOAc as mobile phase to give the pure product (**7**) that was confirmed by ^{1}H NMR, GCMS and elemental analysis (Entry 4 in Supporting Information Table S5 and Figures S49−S52).

(*iv*). In typical catalysis run, a mixture of the phenylacetylene (1.00 mmol) was taken with [{(2,6-*t*-Bu$_2$-C$_6$H$_3$O)(NCy$_2$)}methylidene]Au(C≡CC$_6$H$_5$) (**1**) (0.005 mmol, 0.5 mol %) CH$_3$CN (*ca.* 2 mL) in reaction vial and kept at 80 °C and after 5 minutes formaldehyde (4.00 mmol) and morpholine (1.20 mmol) was added to it. Reaction mixture was stirred for the 24 hours at 80 °C. Afterward, it was cooled to room temperature and volatiles were evaporated and obtained residue was purified by column chromatography using neutral alumina as the stationary phase and mixed medium of petroleum ether and EtOAc as mobile phase to give the pure product (**7**) that was confirmed by ^{1}H NMR, GCMS and elemental analysis (Entry 6 in Supporting Information Table S5 and Figures S49−S52).

(*v*). In typical catalysis run, a mixture of the phenylacetylene (1.00 mmol) was taken with [1,3-*bis*(mesityl)imidazol-2-ylidene]AuCl (0.005 mmol, 0.5 mol %) in CH$_3$CN (*ca.* 2 mL) in reaction vial and kept at 80 °C and after 5 minutes formaldehyde (4.00 mmol) and morpholine (1.20 mmol) was added to it. Reaction mixture was stirred for the 24 hours at 80 °C. Afterward, it was cooled to room temperature and volatiles were evaporated and obtained residue was purified by column chromatography using neutral alumina as the stationary phase and mixed medium of petroleum ether and EtOAc as mobile phase to give the pure product (**7**) that was confirmed by ^{1}H NMR, GCMS and elemental analysis (Entry 8 in Supporting Information Table S5 and Figures S49−S52).

(*vi*). In typical catalysis run, a mixture of the phenylacetylene (1.00 mmol) was taken with [1,3-*bis*(2,6-diisopropylphenyl)imidazol-2-ylidene]AuCl (0.005 mmol, 0.5 mol %) in CH$_3$CN (*ca.* 2 mL) in reaction vial and kept at 80 °C and after 5 minutes formaldehyde (4.00 mmol) and morpholine (1.20 mmol) was added to it. Reaction mixture was stirred for the 24 hours at 80 °C. Afterward, it was cooled to room temperature and volatiles were evaporated and obtained residue was purified by column chromatography using neutral alumina as the stationary phase and mixed medium of petroleum ether and EtOAc as mobile phase to give the pure product (**7**) that was confirmed by ^{1}H NMR, GCMS and elemental analysis (Entry 9 in Supporting Information Table S5 and Figures S49−S52).

(*vii*). In typical catalysis run, a mixture of the phenylacetylene (1.00 mmol) was taken with [2,6-bis-(1-(1S)-menthyl-3-methylene-imidazol-2-ylidene)-pyridine]Au$_2$Cl$_2$ (0.005 mmol, 0.5 mol %) in CH$_3$CN (*ca.* 2 mL) in reaction vial and kept at 80 °C and after 5 minutes formaldehyde (4.00 mmol) and morpholine (1.20 mmol) was added to it. Reaction mixture was stirred for the 24 hours at 80 °C. Afterward, it was cooled to room temperature and volatiles were evaporated and obtained residue was purified by column chromatography using neutral alumina as the stationary phase and mixed medium of petroleum ether and EtOAc as mobile phase to give the pure product (**7**) that was confirmed by ^{1}H NMR, GCMS and elemental analysis (Entry 10 in Supporting Information Table S5 and Figures S49−S52).

General procedure for the Hg drop experiment

(*i*). In a typical Hg-drop experiment, a mixture of the phenylacetylene (1.00 mmol) was taken with [{(2,6-*t*-Bu$_2$-C$_6$H$_3$O)(NCy$_2$)}methylidene]AuCl (0.005 mmol, 0.5 mol %) in CH$_3$CN (*ca.* 2 mL) along with one drop of Hg in reaction vial and kept at 80 °C and after 5 minutes formaldehyde (4.00 mmol) and morpholine (1.20 mmol) was added to it. Reaction mixture was stirred for the 24 hours at 80 °C. Afterward, it was cooled to room temperature and volatiles were evaporated and obtained residue was purified by column chromatography using neutral alumina as the stationary phase and mixed medium of petroleum ether and EtOAc as mobile phase to give the pure product (**7**) that was confirmed by ^{1}H NMR, GCMS and elemental analysis. (Entry 5 in Supporting Information Table S5 and Figures S49−S52).

(*ii*). In a typical Hg-drop experiment, a mixture of the phenylacetylene (1.00 mmol) was taken with [{(2,6-*t*-Bu$_2$-C$_6$H$_3$O)(NCy$_2$)}methylidene]Au(C≡CC$_6$H$_5$) (**1**) (0.005 mmol, 0.5 mol %) in CH$_3$CN (*ca.* 2 mL) along with one drop of Hg in reaction vial and kept at 80 °C and after 5 minutes formaldehyde (4.00 mmol) and morpholine (1.20 mmol) was added to it. Reaction mixture was stirred for the 24 hours at 80 °C. Afterward, it was cooled to room temperature and volatiles were evaporated and obtained residue was purified by column chromatography using neutral alumina as the stationary phase and mixed medium of petroleum ether and EtOAc as mobile phase to give the pure product (**7**) that was confirmed by ^{1}H NMR, GCMS and elemental analysis. (Entry 7 in Supporting Information Table S5 and Figures S49−S52).

General procedure of mass experiment for the detection of the catalytic intermediates

(*i*). In the typical mass experiment, the species {[{(2,6-*t*-Bu$_2$-C$_6$H$_3$O)(NCy$_2$)}methylidene]AuCl(HC≡CPh)} (**1**−**B'**), detected in the reaction mixture of [{(2,6-*t*-Bu$_2$-C$_6$H$_3$O)(NCy$_2$)}methylidene]AuCl (0.005 mmol, 0.5 mol %) and phenylacetylene (1.00 mmol), *ca.* 2 mL of CH$_3$CN at room temperature (Fig. 4 and Supporting Information Figures S117).

(*ii*). In the typical mass experiment, the species {[{(2,6-*t*-Bu$_2$-C$_6$H$_3$O)(NCy$_2$)}methylidene]Au(C≡CPh)} species (**1**), detected in the reaction mixture of [{(2,6-*t*-Bu$_2$-C$_6$H$_3$O)(NCy$_2$)}methylidene]AuCl (0.005 mmol, 0.5 mol %), phenylacetylene (1.00 mmol), formaldehyde (1.20 mmol) and morpholine (1.20 mmol), *ca.* 2 mL of CH$_3$CN at room temperature (Fig. 5 and Supporting Information Figures S118).

(*iii*). In the typical mass experiment, the species {[{(2,4,6-*t*-Bu$_3$-C$_6$H$_2$O)(NCy$_2$)}methylidene]Au(C≡CPh)} species (**4**), detected in the reaction mixture of [{(2,4,6-*t*-Bu$_3$-C$_6$H$_2$O)(NCy$_2$)}methylidene]AuCl (0.005 mmol, 0.5 mol %), phenylacetylene (1.00 mmol), formaldehyde (1.20 mmol) and morpholine (1.20 mmol), *ca.* 2 mL of CH$_3$CN at room temperature (Supporting Information Figures S119 and S120).

General procedure for the X-ray Photoelectron Spectroscopy experiment

The following XPS experiments were performed

(*i*). The XPS experiment conducted for the precatalyst [{(2,4,6-*t*-Bu$_3$-C$_6$H$_2$O)(NCy$_2$)}methylidene]Au(C≡CC$_6$H$_5$) (**4**) itself (Fig. 6 and Supporting Information Figure S121).

(*ii*). In the XPS experiment, a mixture of the [{(2,4,6-*t*-Bu$_3$-C$_6$H$_2$O)(NCy$_2$)}methylidene]Au(C≡CC$_6$H$_5$) (**4**) (0.005 mmol), benzaldehyde (1.20 mmol) and morpholine (1.20 mmol) in CH$_3$CN (*ca.* 2 mL) at room temperature for the 5 minutes. Afterward, the volatiles were evaporated, and the residue was dried under vacuum. The crude material so obtained was used for the XPS analysis (Fig. 6 and Supporting Information Figure S122).

(*iii*). In the XPS experiment, a mixture of the terminal alkynes (1.00 mmol) was taken with [{(2,4,6-*t*-Bu$_3$-C$_6$H$_2$O)(NCy$_2$)}methylidene]Au(C≡CC$_6$H$_5$) (**4**) (0.005 mmol) in CH$_3$CN (*ca.* 2 mL) in reaction vial and

kept at 80 °C and after 5 minutes benzaldehyde (1.20 mmol) and morpholine (1.20 mmol) was added to it. Reaction mixture was stirred for the 24 hours at 80 °C. Afterward, it was cooled to room temperature and volatiles were evaporated, and the residue was dried under vacuum. The crude material so obtained was used for the XPS analysis (Fig. 6 and Supporting Information Figure S123).

General procedure for the synthesis of propargylamine catalyzed by acetylide and chloro derivative of gold(I) acyclic aminooxy carbene complexes

In typical catalysis run, a mixture of the terminal alkynes (1.00 mmol) was taken with [{(2,6-*t*-Bu_2-C_6H_3O)(NCy_2)}methylidene]Au(C≡CC_6H_5) (**1**)/ [{(2,6-*t*-Bu_2-C_6H_3O)(NCy_2)}methylidene]AuCl/ [{(2,4,6-*t*-Bu_3-C_6H_2O)(NCy_2)}methylidene]Au(C≡CC_6H_5) (**4**)/ [{(2,4,6-*t*-Bu_3-C_6H_2O)(NCy_2)}methylidene]AuCl (0.005 mmol, 0.5 mol %) in CH_3CN (*ca.* 2 mL) in reaction vial and kept at 80 °C and after 5 minutes formaldehyde (4.00 mmol)/ (benzaldehyde/ cyclohexanecarboxylde hyde/ cyclopentanecarboxyldehyde) (1.20 mmol) and *sec* amines (1.20 mmol) was added to it. Reaction mixture was stirred for the 24 hours at 80 °C. Afterward, it was cooled to room temperature and volatiles were evaporated and obtained residue was purified by column chromatography using neutral alumina as the stationary phase and mixed medium of petroleum ether and EtOAc as mobile phase to give the pure products (**7**−**18**) (Table 2) that was confirmed by ^{1}H NMR, GCMS and elemental analysis (Supporting Information Figures S49−S96). The characterization data of compounds (**7**−**18**) have been showed in Figures 11−22.

4-(3-phenylprop-2-yn-1-yl)morpholine (7) [64,94]

Yields: 0.188 g, 93 % (**1**), 0.197 g, 98 % (**2**), 0.194 g, 96 % (**3**), 0.193 g, 96 % (**4**), 0.199 g, 99 % (**5**), 0.197 g, 98 % (**6**).

^{1}H NMR ($CDCl_3$, 400 MHz, 25°C): δ ppm, 7.44−7.42 (m, 2H, $C_6\underline{H}_5$), 7.30−7.28 (m, 3H, $C_6\underline{H}_5$), 3.77 (t, 4H, $^3J_{HH}$ = 4 Hz, $NC_4\underline{H}_8O$), 3.50 (s, 2H, C$\underline{H}_2$), 2.64 (t, 4H, $^3J_{HH}$ = 4 Hz, $NC_4\underline{H}_8O$). GCMS (ESI): $[M]^+$ *m/z* = 201.1. Anal. Calcd. for $C_{13}H_{15}NO$: C, 77.58; H, 7.51; N, 6.96; Found: C, 76.79; H, 6.77; N, 6.11 %.

4-(3-(p-tolyl)prop-2-yn-1-yl)morpholine (8) [64,94]

Yields: 0.212 g, 98 % (**1**), 0.211 g, 98 % (**4**).

^{1}H NMR ($CDCl_3$, 400 MHz, 25°C): δ ppm, 7.31 (d, 2H, $^3J_{HH}$ = 8 Hz, *o*-$C_6\underline{H}_4CH_3$), 7.08 (d, 2H, $^3J_{HH}$ = 8 Hz, *m*-$C_6\underline{H}_4CH_3$), 3.75 (t, 4H, $^3J_{HH}$ = 5 Hz, $NC_4\underline{H}_8O$), 3.47 (s, 2H, C$\underline{H}_2$), 2.62 (t, 4H, $^3J_{HH}$ = 5 Hz, $NC_4\underline{H}_8O$), 2.32 (s, 3H, $C_6H_4C\underline{H}_3$). GCMS (ESI): $[M]^+$ *m/z* = 215.2. Anal. Calcd. for $C_{14}H_{17}NO$: C, 78.10; H, 7.96; N, 6.51; Found: C, 77.30; H, 7.89; N, 6.04 %.

4-(3-(4-phenoxyphenyl)prop-2-yn-1-yl)morpholine (9) [64,94]

Yields: 0.291 g, 99 % (**1**), 0.278 g, 95 % (**4**).

^{1}H NMR ($CDCl_3$, 400 MHz, 25°C): δ ppm, 7.44−7.41 (m, 2H, *o*-$C_6\underline{H}_5$), 7.40−7.35 (m, 2H, *m*-$C_6\underline{H}_5$), 7.18−7.14 (m, 1H, *p*-$C_6\underline{H}_5$), 7.05−7.03 (m, 2H, *o*-$C_6\underline{H}_4$), 6.96−6.92 (m, 2H, *m*-$C_6\underline{H}_4$), 3.80 (t, 4H, $^3J_{HH}$ = 5 Hz, $NC_4\underline{H}_8O$), 3.52 (s, 2H, C$\underline{H}_2$), 2.67 (t, 4H, $^3J_{HH}$ = 5 Hz, $NC_4\underline{H}_8O$). GCMS (ESI): $[M]^+$ *m/z* = 293.1. Anal. Calcd. for $C_{19}H_{19}NO_2$: C, 77.79; H, 6.53; N, 4.77; Found: C, 76.94; H, 6.71; N, 4.08 %.

1-(3-phenylprop-2-yn-1-yl)piperidine (10) [64,94]

Yields: 0.187 g, 94 % (**1**), 0.191 g, 96 % (**4**).

^{1}H NMR ($CDCl_3$, 400 MHz, 25°C): δ ppm, 7.44−7.42 (m, 2H, $C_6\underline{H}_5$), 7.30−7.28 (m, 3H, $C_6\underline{H}_5$), 3.49 (s, 2H, C$\underline{H}_2$), 2.59 (s, 4H, $NC_5\underline{H}_{10}$), 1.69−1.64 (m, 4H, $NC_5\underline{H}_{10}$), 1.49 (br, 2H, $NC_5\underline{H}_{10}$). GCMS (ESI): $[M]^+$ *m/z* = 198.2. Anal. Calcd. for $C_{14}H_{17}N$: C, 84.37; H, 8.60; N, 7.03; Found: C, 84.97; H, 8.88; N, 6.51 %.

1-(3-(p-tolyl)prop-2-yn-1-yl)piperidine (11) [64,94]

Yields: 0.202 g, 95 % (**1**), 0.209 g, 98 % (**4**).

^{1}H NMR ($CDCl_3$, 400 MHz, 25°C): δ ppm, 7.35 (d, 2H, $^3J_{HH}$ = 8 Hz, *o*-$C_6\underline{H}_4CH_3$), 7.12 (d, 2H, $^3J_{HH}$ = 8 Hz, *m*-$C_6\underline{H}_4CH_3$), 3.49 (s, 2H, C$\underline{H}_2$), 2.59 (s, 4H, $NC_5\underline{H}_{10}$), 2.36 (s, 3H, $C_6H_4C\underline{H}_3$), 1.69−1.64 (m, 4H, $NC_5\underline{H}_{10}$), 1.47 (br, 2H, $NC_5\underline{H}_{10}$). GCMS (ESI): $[M]^+$ *m/z* = 212.2. Anal. Calcd. for $C_{15}H_{19}N$: C, 84.46; H, 8.98; N, 6.57; Found: C, 84.52; H, 9.30; N, 5.90 %.

1-(3-(4-phenoxyphenyl)prop-2-yn-1-yl)piperidine (12) [64,94]

Yields: 0.272 g, 93 % (**1**), 0.276 g, 95 % (**4**).

^{1}H NMR ($CDCl_3$, 400 MHz, 25°C): δ ppm, 7.42 (d, 2H, $^3J_{HH}$ = 9 Hz, *o*-$C_6\underline{H}_5$), 7.37 (t, 2H, $^3J_{HH}$ = 8 Hz, *m*-$C_6\underline{H}_5$), 7.15 (t, 1H, $^3J_{HH}$ = 8 Hz, *m*-$C_6\underline{H}_5$), 7.04 (d, 2H, $^3J_{HH}$ = 9 Hz, *o*-$C_6\underline{H}_4$), 6.94 (d, 2H, $^3J_{HH}$ = 9 Hz, *m*-$C_6\underline{H}_4$), 3.49 (s, 2H, C$\underline{H}_2$), 2.59 (s, 4H, $NC_5\underline{H}_{10}$), 1.67−1.64 (m, 4H, $NC_5\underline{H}_{10}$), 1.47 (br, 2H, $NC_5\underline{H}_{10}$). GCMS (ESI): $[M]^+$ *m/z* = 291.1. Anal. Calcd. for $C_{20}H_{21}NO$: C, 82.44; H, 7.26; N, 4.81; Found: C, 82.44; H, 7.31; N, 3.87 %.

4-(1,3-diphenylprop-2-yn-1-yl)morpholine (13) [95]

Yields: 0.052 g, 19 % (**1**), 0.120 g, 43 % (**4**).

^{1}H NMR ($CDCl_3$, 400 MHz, 25°C): δ ppm, 7.64 (d, 2H, $^3J_{HH}$ = 7 Hz, $C_6\underline{H}_5$), 7.54−7.52 (m, 2H, $C_6\underline{H}_5$), 7.39−7.29 (m, 6H, $2C_6\underline{H}_5$), 4.80 (s, 1H, C$\underline{H}$), 3.79−3.70 (m, 4H, $NC_4\underline{H}_8O$), 2.65 (s, 4H, $NC_4\underline{H}_8O$). GCMS (ESI): $[M]^+$ *m/z* = 277.1. Anal. Calcd. for $C_{19}H_{19}NO$: C, 82.28; H, 6.90; N, 5.05; Found: C, 81.69; H, 6.92; N, 4.49 %.

4-(1-phenyl-3-(p-tolyl)prop-2-yn-1-yl)morpholine (14) [95]

Yields: 0.105 g, 36 % (**1**), 0.139 g, 47 % (**4**).

^{1}H NMR ($CDCl_3$, 400 MHz, 25°C): δ ppm, 7.63 (d, 2H, $^3J_{HH}$ = 8 Hz, $C_6\underline{H}_5$), 7.41 (d, 2H, $^3J_{HH}$ = 8 Hz, $C_6\underline{H}_4CH_3$), 7.36 (t, 2H, $^3J_{HH}$ = 8 Hz, $C_6\underline{H}_5$), 7.29 (t, 1H, $^3J_{HH}$ = 7 Hz, $C_6\underline{H}_5$), 7.13 (d, 2H, $^3J_{HH}$ = 8 Hz, $C_6\underline{H}_4CH_3$), 4.77 (s, 1H, C$\underline{H}$), 3.77−3.68 (m, 4H, $NC_4\underline{H}_8O$), 2.67−2.59 (m, 4H, $NC_4\underline{H}_8O$), 2.39 (s, 3H, $C_6H_4C\underline{H}_3$). GCMS (ESI): $[M]^+$ *m/z* = 291.1. Anal. Calcd. for $C_{20}H_{21}NO$: C, 82.44; H, 7.26; N, 4.81; Found: C, 83.03; H, 7.72; N, 4.00 %.

4-(1-cyclopentyl-3-phenylprop-2-yn-1-yl)morpholine (15) [95]

Yields: 0.146 g, 54 % (**1**), 0.149 g, 55 % (**4**).

^{1}H NMR ($CDCl_3$, 400 MHz, 25°C): δ ppm, 7.48−7.44 (m, 2H, $C_6\underline{H}_5$), 7.35−7.30 (m, 3H, $C_6\underline{H}_5$), 3.82−3.73 (m, 4H, $NC_4\underline{H}_8O$), 3.25 (d, 1H, $^3J_{HH}$ = 10 Hz, C$\underline{H}$), 2.79−2.74 (m, 2H, $NC_4\underline{H}_8O$), 2.59−2.54 (m, 2H, $NC_4\underline{H}_8O$), 2.30−2.22 (m, 1H, $C_5\underline{H}_9$), 1.96−1.88 (m, 1H, $C_5\underline{H}_9$), 1.84−1.76 (m, 1H, $C_5\underline{H}_9$), 1.67−1.49 (m, 6H, $C_5\underline{H}_9$). GCMS (ESI): $[M]^+$ *m/z* = 268.1. Anal. Calcd. for $C_{18}H_{23}NO$: C, 80.26; H, 8.61; N, 5.20; Found: C, 79.74; H, 8.82; N, 4.36 %.

4-(1-cyclopentyl-3-(p-tolyl)prop-2-yn-1-yl)morpholine (16) [95]

Yields: 0.178 g, 63 % (**1**), 0.208 g, 73 % (**4**).

^{1}H NMR ($CDCl_3$, 400 MHz, 25°C): δ ppm, 7.35 (d, 2H, $^3J_{HH}$ = 8 Hz, *o*-$C_6\underline{H}_4CH_3$), 7.13 (d, 2H, $^3J_{HH}$ = 8 Hz, *m*-$C_6\underline{H}_4CH_3$), 3.81−3.71 (m, 4H, $NC_4\underline{H}_8O$), 3.24 (d, 1H, $^3J_{HH}$ = 10 Hz, C$\underline{H}$), 2.79−2.73 (m, 2H, $NC_4\underline{H}_8O$), 2.58−2.53 (m, 2H, $NC_4\underline{H}_8O$), 2.37 (s, 3H, $C_6H_4C\underline{H}_3$), 2.27−2.21 (m, 1H, $C_5\underline{H}_9$), 1.94−1.90 (m, 1H, $C_5\underline{H}_9$), 1.81−1.75 (m, 1H, $C_5\underline{H}_9$), 1.67−1.49 (m, 6H, $C_5\underline{H}_9$). GCMS (ESI): $[M]^+$ *m/z* = 282.1. Anal. Calcd. for $C_{19}H_{25}NO$: C, 80.52; H, 8.89; N, 4.94; Found: C, 80.40; H, 8.92; N, 3.97 %.

4-(1-cyclohexyl-3-phenylprop-2-yn-1-yl)morpholine (17) [95]

Yields: 0.226 g, 80 % (**1**), 0.223 g, 78 % (**4**).

^{1}H NMR ($CDCl_3$, 400 MHz, 25°C): δ ppm, 7.47−7.45 (m, 2H, $C_6\underline{H}_5$), 7.32−7.31 (m, 3H, $C_6\underline{H}_5$), 3.80−3.72 (m, 4H, $NC_4\underline{H}_8O$), 3.15 (d, 1H, $^3J_{HH}$ = 10 Hz, C$\underline{H}$), 2.74−2.70 (m, 2H, $NC_4\underline{H}_8O$), 2.56−2.51 (m, 2H, $NC_4\underline{H}_8O$), 2.14−2.05 (m, 2H, $C_6\underline{H}_{11}$), 1.78−1.61 (m, 4H, $C_6\underline{H}_{11}$), 1.32−1.22 (m, 3H, $C_6\underline{H}_{11}$), 1.12−0.97 (m, 2H, $C_6\underline{H}_{11}$). GCMS (ESI): $[M]^+$ *m/z* = 282.1. Anal. Calcd. for $C_{19}H_{25}NO$: C, 80.52.58; H, 8.89; N, 4.94; Found: C, 80.41; H, 8.89; N, 4.35 %.

4-(1-cyclohexyl-3-(p-tolyl)prop-2-yn-1-yl)morpholine (18) [95]

Yields: 0.254 g, 85 % (**1**), 0.277 g, 93 % (**4**).

^{1}H NMR ($CDCl_3$, 400 MHz, 25°C): δ ppm, 7.35 (d, 2H, $^3J_{HH}$ = 8 Hz, *o*-$C_6\underline{H}_4CH_3$), 7.12 (d, 2H, $^3J_{HH}$ = 8 Hz, *m*-$C_6\underline{H}_4CH_3$), 3.81−3.71 (m, 4H, $NC_4\underline{H}_8O$), 3.14 (d, 1H, $^3J_{HH}$ = 10 Hz, C$\underline{H}$), 2.74−2.69 (m, 2H, $NC_4\underline{H}_8O$), 2.55−2.50 (m, 2H, $NC_4\underline{H}_8O$), 2.36 (s, 3H, $C_6H_4C\underline{H}_3$), 2.14−2.04 (m, 2H, $C_6\underline{H}_{11}$), 1.81−1.60 (m, 4H, $C_6\underline{H}_{11}$), 1.32−1.19 (m, 3H, $C_6\underline{H}_{11}$), 1.11−0.97 (m, 2H, $C_6\underline{H}_{11}$). GCMS (ESI): $[M]^+$ *m/z* = 296.1. Anal. Calcd. for $C_{20}H_{27}NO$: C, 80.76; H, 9.15; N, 4.71; Found: C, 80.66; H, 9.08; N, 4.31 %.

General procedure for the synthesis of amino indolizines catalyzed by acetylide and chloro derivative of gold(I) acyclic aminooxy carbene complexes

(i) In typical catalysis run, a mixture of the terminal alkynes (1.00 mmol) was taken with [{(2,6-*t*-Bu_2-C_6H_3O)(NCy_2)}methylidene]Au(C≡CC_6H_5) (**1**)/ [{(2,6-*t*-Bu_2-C_6H_3O)(NCy_2)}methylidene]AuCl (0.01 mmol, 1 mol %) and $AgBF_4$ (0.01 mmol, 1 mol %) in *ca.* 2 mL CH_3CN in reaction vial and kept at 80 °C and after 5 minutes pyridine-2-carboxyldehyde (1.20 mmol) and morpholine (1.20 mmol) was added to it. Reaction mixture was stirred for the 24 hours at 80 °C. Afterward, it was cooled to room temperature and volatiles were evaporated and obtained residue was purified by column chromatography using neutral alumina as the stationary phase and mixed medium of petroleum ether and EtOAc as mobile phase to give the pure products (**19**−**23**) (Table 3) that was confirmed by ^{1}H NMR, HRMS and elemental analysis (Supporting Information Figures S97−S116). The characterization data of compounds (**19**−**23**) is shown in Figures 23−27.

4-(3-phenylindolizin-1-yl)morpholine (19) [95]

Yield: 0.154 g, 55 % (**1**).

^{1}H NMR ($CDCl_3$, 400 MHz, 25°C): δ ppm, 8.22 (d, 1H, $^3J_{HH}$ = 7 Hz, $C_5\underline{H}_4N$), 7.57 (d, 2H, $^3J_{HH}$ = 8 Hz, *o*-$C_6\underline{H}_5$), 7.50−7.45 (m, 3H, $C_5\underline{H}_4N$ and *m*-$C_6\underline{H}_5$), 7.34 (t, 1H, $^3J_{HH}$ = 8 Hz, *p*-$C_6\underline{H}_5$), 6.73 (s, 1H, $C_4\underline{H}N$), 6.59 (t, 1H, $^3J_{HH}$ = 8 Hz, $C_5\underline{H}_4N$), 6.44 (t, 1H, $^3J_{HH}$ = 7 Hz, $C_5\underline{H}_4N$), 3.94 (t, 4H, $^3J_{HH}$ = 5 Hz, $NC_4\underline{H}_8O$), 3.08 (s, 4H, $NC_4\underline{H}_8O$). HRMS (ESI): calcd. for $[C_{18}H_{18}N_2O + H]^+$ *m/z* 279.1492; found *m/z* 279.1442. Anal. Calcd. for $C_{18}H_{18}N_2O$: C, 77.67; H, 6.52; N, 10.06; Found: C, 77.41; H, 6.77; N, 9.48 %.

4-(3-(p-tolyl)indolizin-1-yl)morpholine (20) [95]

Yield: 0.196 g, 67 % (**1**).

^{1}H NMR ($CDCl_3$, 400 MHz, 25°C): δ ppm, 8.19 (br, 1H, $C_5\underline{H}_4N$), 7.48−7.45 (m, 3H, $C_5\underline{H}_4N$ and *o*-$C_6\underline{H}_4$), 7.30 (d, 2H, $^3J_{HH}$ = 8 Hz, *m*-$C_6\underline{H}_4$), 6.70 (s, 1H, $C_4\underline{H}N$), 6.57 (br, 1H, $C_5\underline{H}_4N$), 6.42 (br, 1H, $C_5\underline{H}_4N$), 3.94 (t, 4H, $^3J_{HH}$ = 4 Hz, $NC_4\underline{H}_8O$), 3.09 (s, 4H, $NC_4\underline{H}_8O$), 2.44 (s, 3H, $C\underline{H}_3$). HRMS (ESI): calcd. for $[C_{19}H_{20}N_2O + H]^+$ *m/z* 293.1648; found *m/z* 293.1617. Anal. Calcd. for $C_{19}H_{20}N_2O$: C, 78.05; H, 6.90; N, 9.58; Found: C, 77.33; H, 6.28; N, 9.16 %.

4-(3-(4-phenoxyphenyl)indolizin-1-yl)morpholine (21) [95]

Yield: 0.224 g, 60 % (**1**).

^{1}H NMR ($CDCl_3$, 400 MHz, 25°C): δ ppm, 8.16 (d, 1H, $^3J_{HH}$ = 7 Hz, $C_5\underline{H}_4N$), 7.52 (d, 2H, $^3J_{HH}$ = 8 Hz, *o*-$C_6\underline{H}_4$), 7.45 (d, 1H, $^3J_{HH}$ = 9 Hz, $C_5\underline{H}_4N$), 7.40 (t, 2H, $^3J_{HH}$ = 8 Hz, *m*-$C_6\underline{H}_5$), 7.16 (t, 2H, $^3J_{HH}$ = 8 Hz, *p*-$C_6\underline{H}_5$), 7.13−7.09 (m, 4H, *m*-$C_6\underline{H}_4$ and *o*-$C_6\underline{H}_5$), 6.69 (s, 1H, $C_4\underline{H}N$), 6.58 (t, 1H, $^3J_{HH}$ = 8 Hz, $C_5\underline{H}_4N$), 6.44 (t, 1H, $^3J_{HH}$ = 7 Hz, $C_5\underline{H}_4N$), 3.94 (t, 4H, $^3J_{HH}$ = 5 Hz, $NC_4\underline{H}_8O$), 3.08 (t, 4H, $^3J_{HH}$ = 5 Hz, $NC_4\underline{H}_8O$). HRMS (ESI): calcd. for $[C_{24}H_{22}N_2O_2 + H]^+$ *m/z* 371.1754; found *m/z* 371.1781. Anal. Calcd. for $C_{24}H_{22}N_2O_2$: C, 77.81; H, 5.99; N, 7.56; Found: C, 77.69; H, 5.48; N, 7.44 %.

4-(3-(4-chlorophenyl)indolizin-1-yl)morpholine (22) [95]

Yield: 0.228 g, 73 % (**1**).

^{1}H NMR ($CDCl_3$, 400 MHz, 25°C): δ ppm, 8.15 (d, 1H, $^3J_{HH}$ = 7 Hz, $C_5\underline{H}_4N$), 7.51−7.43 (m, 5H, $C_5\underline{H}_4N$ and $C_6\underline{H}_4$), 6.70 (s, 1H, $C_4\underline{H}N$), 6.62−6.58 (m, 1H, $C_5\underline{H}_4N$), 6.48−7.44 (m, 1H, $C_5\underline{H}_4N$), 3.94 (t, 4H, $^3J_{HH}$ = 5 Hz, $NC_4\underline{H}_8O$), 3.07 (t, 4H, $^3J_{HH}$ = 5 Hz, $NC_4\underline{H}_8O$). HRMS (ESI): calcd. for $[C_{18}H_{17}ClN_2O + H]^+$ *m/z* 313.1102; found *m/z* 313.1125. Anal. Calcd. for $C_{18}H_{17}ClN_2O$: C, 69.12; H, 5.48; N, 8.96; Found: C, 69.73; H, 6.40; N, 8.16 %.

4-(3-(4-bromophenyl)indolizin-1-yl)morpholine (23) [95]

Yield: 0.175 g, 49 % (**1**).

^{1}H NMR ($CDCl_3$, 400 MHz, 25°C): δ ppm, 8.11 (d, 1H, $^3J_{HH}$ = 7 Hz, $C_5\underline{H}_4N$), 7.59−7.57 (m, 2H, $C_6\underline{H}_4$), 7.46−7.41 (m, 3H, $C_5\underline{H}_4N$ and $C_6\underline{H}_4$), 6.67 (s, 1H, $C_4\underline{H}N$), 6.60−6.56 (m, 1H, $C_5\underline{H}_4N$), 6.45−7.42 (m, 1H, $C_5\underline{H}_4N$), 3.91 (t, 4H, $^3J_{HH}$ = 5 Hz, $NC_4\underline{H}_8O$), 3.04 (t, 4H, $^3J_{HH}$ = 5 Hz, $NC_4\underline{H}_8O$). HRMS (ESI): calcd. for $[C_{18}H_{17}BrN_2O + H]^+$ *m/z* 357.0597; found *m/z* 357.0556. Anal. Calcd. for $C_{18}H_{17}BrN_2O$: C, 60.52; H, 4.80; N, 7.84; Found: C, 60.17; H, 5.73; N, 7.84 %. (Fig. 11,Fig. 12,Fig. 13,

4-(3-phenylprop-2-yn-1-yl)morpholine (7)[32, 54]

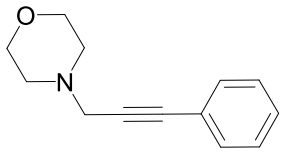

(**7**)

Fig. 11. The characterization data of (**7**).

4-(3-(p-tolyl)prop-2-yn-1-yl)morpholine (8)[32, 54]

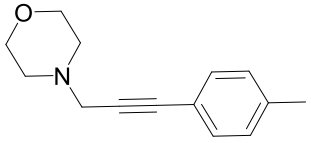

(**8**)

Fig. 12. The characterization data of (**8**).

4-(3-(4-phenoxyphenyl)prop-2-yn-1-yl)morpholine (9)[32, 54]

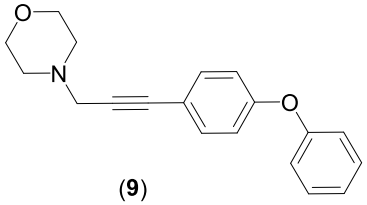

(**9**)

Fig. 13. The characterization data of (**9**).

1-(3-phenylprop-2-yn-1-yl)piperidine (10)[32, 54]

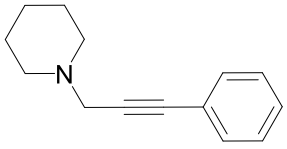

(**10**)

Fig. 14. The characterization data of (**10**).

1-(3-(p-tolyl)prop-2-yn-1-yl)piperidine (11)[32, 54]

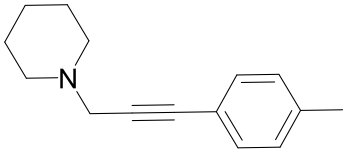

(**11**)

Fig. 15. The characterization data of (**11**).

1-(3-(4-phenoxyphenyl)prop-2-yn-1-yl)piperidine (12)[32, 54]

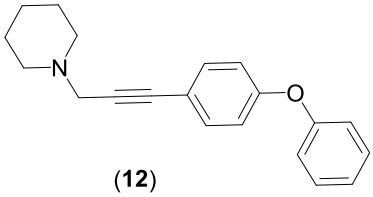

(**12**)

Fig. 16. The characterization data of (**12**).

4-(1,3-diphenylprop-2-yn-1-yl)morpholine (13)[55]

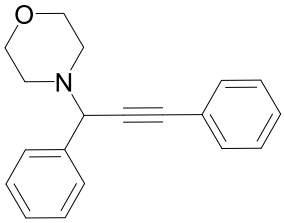

(**13**)

Fig. 17. The characterization data of (**13**).

4-(1-phenyl-3-(p-tolyl)prop-2-yn-1-yl)morpholine (14)[55]

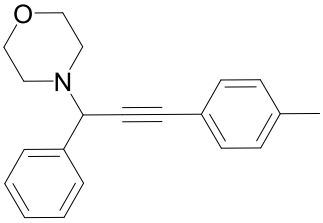

(**14**)

Fig. 18. The characterization data of (**14**).

4-(1-cyclopentyl-3-phenylprop-2-yn-1-yl)morpholine (15)[55]

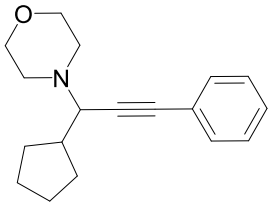

(**15**)

Fig. 19. The characterization data of (**15**).

4-(1-cyclopentyl-3-(p-tolyl)prop-2-yn-1-yl)morpholine (16)[55]

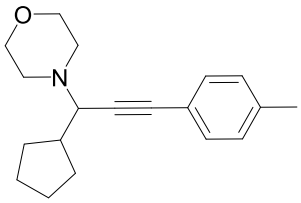

(**16**)

Fig. 20. The characterization data of (**16**).

4-(1-cyclohexyl-3-phenylprop-2-yn-1-yl)morpholine (17)[55]

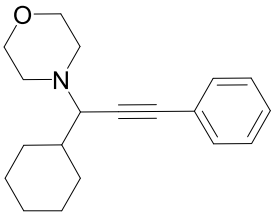

(**17**)

Fig. 21. The characterization data of (**17**).

4-(1-cyclohexyl-3-(p-tolyl)prop-2-yn-1-yl)morpholine (18)[55]

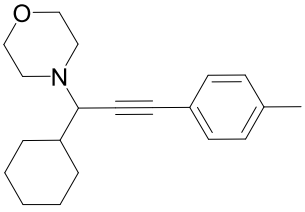

(**18**)

Fig. 22. The characterization data of (**18**).

Fig. 14,Fig. 15,Fig. 16,Fig. 17,Fig. 18,Fig. 19,Fig. 20,Fig. 21,Fig. 22, Fig. 23,Fig. 24,Fig. 25,Fig. 26,Fig. 27).

Computational Details

In this study, Gaussian 16 Revision D.01 [70] was used for performing all DFT calculations, while Orca 4.2.1 version software [79, 80] was chosen specifically for spectroscopic calculations, including ^{13}C NMR analyses. Grimme's dispersion-corrected B3LYP functional (B3LYP-D3) was employed for geometry optimization [71,72]. The calculations were conducted using the SDD basis set for gold metal [73] and the 6-31G* basis set for elements such as C, H, N, O, and Cl [71,72, 74,75] (Supporting Information Table S8-S37). The coordinates of optimised structures are given in Supporting Information Table S13-S41. Frequency calculations were executed to pinpoint minima on the potential-energy surface (PES) and to determine the free energy correction energy. Furthermore, we incorporated solvation energy using the polarizable continuum model (PCM) and acetonitrile solvent [77] into the gas phase energy by employing a more advanced level of theory (B3LYP-D3/def2TZVP) [96]. Furthermore, Gaussian 16 software was utilized to conduct thorough NBO (Natural Bond Orbital) [78] calculations using DFT methods. The NBO analysis offered detailed insights into the characteristics of bonding orbitals and provided valuable information about the distribution of natural charges within the system (Supporting Information Table S9, S10, S11).

We conducted steric map plot calculations using the SambVca 2.0

4-(3-phenylindolizin-1-yl)morpholine (19)[55]

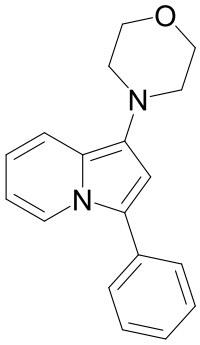

(19)

Fig. 23. The characterization data of (**19**).

4-(3-(p-tolyl)indolizin-1-yl)morpholine (20)[55]

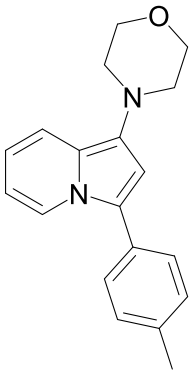

(20)

Fig. 24. The characterization data of (**20**).

tool [89], specifically designed for Analyzing Catalytic Pockets through Topographic Steric Maps. The SambVca 2.0 web tool establishes a correlation between steric effects and the percentage of buried volume (% V_{Bur}). Color transitions from red to blue on the steric map plot indicate a decrease in steric influence, while the reverse trend is denoted by blue to red shifts. For the purpose of conducting ^{13}C NMR calculations using ORCA 4.2.1 software [79,80], we opted for the hybrid Generalized Gradient Approximation (GGA) B3LYP functional [71,72,75]. In our calculations, the resolution of identity (RIJK) approximation [81] has been employed throughout. This RI approximation has been found to be fast for small to medium molecules. We have used basis set combination of Sapporo-DKH3-DZP-2012 for gold(I) metal [82], IGLO-II for the carbon atom [84,85], and for the rest of the atoms, O, N, and H, the DKH-def2-SVP basis set has been considered [76,86,87] for ^{13}C NMR. Optimized coordinates of Gaussian16 software have been used for the ^{13}C NMR calculations. AIM analyses has been done using Multiwfn software.

4-(3-(4-phenoxyphenyl)indolizin-1-yl)morpholine (21)[55]

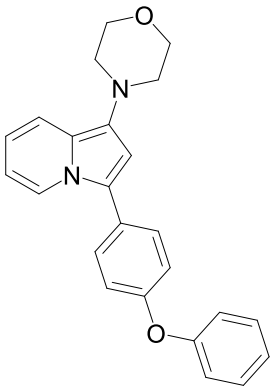

(21)

Fig. 25. The characterization data of (**21**).

4-(3-(4-chlorophenyl)indolizin-1-yl)morpholine (22)[55]

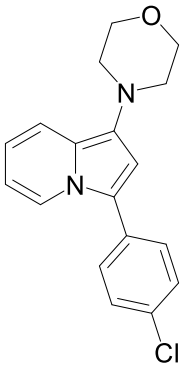

(22)

Fig. 26. The characterization data of (**22**).

4-(3-(4-bromophenyl)indolizin-1-yl)morpholine (23)[55]

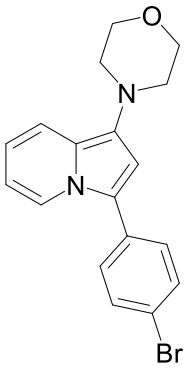

(23)

Fig. 27. The characterization data of (**23**).

CRediT authorship contribution statement

Jyoti Singh: Methodology. **Purva Dua:** Methodology. **Gopalan Rajaraman:** Supervision, Software. **Prasenjit Ghosh:** Writing – review & editing, Writing – original draft, Supervision, Funding acquisition, Conceptualization.

Declaration of competing interest

The authors declare that they have no known competing financial interests or personal relationships that could have appeared to influence the work reported in this paper.

Data availability

No data was used for the research described in the article.

Acknowledgments

We thank the Department of Science and Technology (grant No.: CRG/2019/000029, CRG/2022/001697, and CRG/2023/000012), New Delhi, India, and the Council of Scientific & Industrial Research (CSIR) {01(2880)/17/EMR-II}, and 01/3098/23/EMR II), New Delhi, India, for financial support of this research. We gratefully acknowledge the Single Crystal X-ray Diffraction Facility, Department of Chemistry, IIT Bombay, Mumbai, India, for the crystallographic characterization data. We also gratefully thank the Central Surface Analytical Facility of IIT Bombay, Mumbai, India, for the X-ray Photoelectron Spectroscopy characterization data. J. S. thanks the DST-INSPIRE, New Delhi, India, for the research fellowship. P. D. thanks PMRF for the research fellowship.

Supplementary materials

Supplementary material associated with this article can be found, in the online version, at doi:10.1016/j.mcat.2024.114387.

References

[1] I.T. Trotus, T. Zimmermann, F. Schueth, Catalytic Reactions of Acetylene: A Feedstock for the Chemical Industry Revisited, Chem. Rev. (Washington, DC, U. S.) 114 (3) (2014) 1761–1782.
[2] B. Yang, S. Lu, Y. Wang, S. Zhu, Diverse synthesis of C2-linked functionalized molecules via molecular glue strategy with acetylene, Nat. Commun. 13 (1) (2022) 1858.
[3] J. Comas-Barceló, J.P.A. Harrity, Metal Acetylides in Cycloaddition Reactions, Synthesis. (Mass) 49 (06) (2017) 1168–1181.
[4] S.R. Waldvogel, Comprehensive organic name reactions and reagents, Synthesis. (Mass) 2010 (05) (2010), 892-892.
[5] Name Reactions for Homologation, Part 1, Wiley-Blackwell, Hoboken, NJ, 2009.
[6] N. Kaur, G. Kaur, A review on Homo- and Hetero- coupling reactions, Materials Today: Proceedings 48 (2022) 1283–1300.
[7] I. Kanwal, A. Mujahid, N. Rasool, K. Rizwan, A. Malik, G. Ahmad, S.A. Shah, U. Rashid, N.M. Nasir, Palladium and Copper Catalyzed Sonogashira cross Coupling an Excellent Methodology for C-C Bond Formation over 17 Years: A Review, Catalysts. (2020).
[8] F. Mohjer, P. Mofatehnia, Y. Rangraz, M.M. Heravi, Pd-free, Sonogashira cross-coupling reaction. An update, J. Organomet. Chem. 936 (2021) 121712.
[9] F. Mohajer, M.M. Heravi, V. Zadsirjan, N. Poormohammad, Copper-free Sonogashira cross-coupling reactions: an overview, RSC. Adv. 11 (12) (2021) 6885–6925.
[10] K.V. Arundhathi, P. Vaishnavi, T. Aneeja, G. Anilkumar, Copper-catalyzed Sonogashira reactions: advances and perspectives since 2014, RSC. Adv. 13 (7) (2023) 4823–4834.
[11] H. Ben El Ayouchia, L. Bahsis, H. Anane, L.R. Domingo, S.E. Stiriba, Understanding the mechanism and regioselectivity of the copper(i) catalyzed [3 + 2] cycloaddition reaction between azide and alkyne: a systematic DFT study, RSC. Adv. 8 (14) (2018) 7670–7678.
[12] P. Kalra, R. Kaur, G. Singh, H. Singh, G. Singh, G.Kaur Pawan, J. Singh, Metals as "Click" catalysts for alkyne-azide cycloaddition reactions: An overview, J. Organomet. Chem. 944 (2021) 121846.
[13] P. Saini, G.Singh Sonika, G. Kaur, J. Singh, H. Singh, Robust and Versatile Cu(I) metal frameworks as potential catalysts for azide-alkyne cycloaddition reactions: Review, Molecular Catalysis 504 (2021) 111432.
[14] J. Kaur, M. Saxena, N. Rishi, An Overview of Recent Advances in Biomedical Applications of Click Chemistry, Bioconjug. Chem. 32 (8) (2021) 1455–1471.
[15] B.D. Fairbanks, L.J. Macdougall, S. Mavila, J. Sinha, B.E. Kirkpatrick, K.S. Anseth, C.N. Bowman, Photoclick Chemistry: A Bright Idea, Chem. Rev. 121 (12) (2021) 6915–6990.
[16] A. Suárez, G.C. Fu, A Straightforward and Mild Synthesis of Functionalized 3-Alkynoates, Angewandte Chemie International Edition 43 (27) (2004) 3580–3582.
[17] N. Chen, M. He, T. Zhou, Y. Zhu, H. Zhang, S. Peng, Recent Advances in the Tandem Cyclization/Cycloaddition of Allene Intermediates from Copper-Catalyzed Cross-Coupling of Diazo Compounds with Terminal Alkynes, Synthesis. (Mass) 53 (04) (2020) 611–622.
[18] M.L. Hossain, J. Wang, Cu(I)-Catalyzed Cross-Coupling of Diazo Compounds with Terminal Alkynes: An Efficient Access to Allenes, The Chemical Record 18 (11) (2018) 1548–1559.
[19] R. Yuan, Z. Lin, Mechanism for the Carboxylative Coupling Reaction of a Terminal Alkyne, CO2, and an Allylic Chloride Catalyzed by the Cu(I) Complex: A DFT Study, ACS. Catal. 4 (12) (2014) 4466–4473.
[20] J. Hong, M. Li, J. Zhang, B. Sun, F. Mo, C−H Bond, Carboxylation with Carbon Dioxide, ChemSusChem. 12 (1) (2019) 6–39.
[21] E. Vessally, A. Hosseinian, M. Babazadeh, L. Edjlali, R. Hosseinzadeh-Khanmiri, Metal Catalyzed Carboxylative Coupling of Terminal Alkynes, Organohalides and Carbon Dioxide: A Novel and Promising Synthetic Strategy Toward 2-Alkynoates (A Review), Curr. Org. Chem. 22 (4) (2018) 315–322.
[22] C. Qiao, Y. Cao, L.N. He, Transition Metal-Catalyzed Carboxylation of Terminal Alkynes with CO2, Mini. Rev. Org. Chem. 15 (4) (2018) 283–290.
[23] X. Qi, J.M. Ready, Copper-Promoted Cycloaddition of Diazocarbonyl Compounds and Acetylides, Angewandte Chemie International Edition 46 (18) (2007) 3242–3244.
[24] S. He, L. Chen, Y.N. Niu, L.Y. Wu, Y.M. Liang, 1,3-Dipolar cycloaddition of diazoacetate compounds to terminal alkynes promoted by Zn(OTf)2: an efficient way to the preparation of pyrazoles, Tetrahedron. Lett. 50 (20) (2009) 2443–2445.
[25] U. Grošelj, F. Požgan, B. Štefane, J. Svete, Copper-Catalyzed Azomethine Imine–Alkyne Cycloadditions (CuAIAC), Synthesis. (Mass) 50 (23) (2018) 4501–4524.
[26] A. Deepthi, N.V. Thomas, S.L. Sruthi, An overview of the reactions involving azomethine imines over half a decade, New Journal of Chemistry 45 (20) (2021) 8847–8873.
[27] J. Liu, S. Dasgupta, M.P. Watson, Enantioselective additions of copper acetylides to cyclic iminium and oxocarbenium ions, Beilstein. J. Org. Chem. 11 (2015) 2696–2706.
[28] R.K. Khangarot, K.P. Kaliappan, Kinugasa Reaction: A Direct One-Pot Route to Highly Functionalized β-Lactams, European. J. Org. Chem. 2013 (34) (2013) 7664–7677.
[29] T.C. Malig, D. Yu, J.E. Hein, A Revised Mechanism for the Kinugasa Reaction, J. Am. Chem. Soc. 140 (29) (2018) 9167–9173.
[30] M. Chigrinova, D.A. MacKenzie, A.R. Sherratt, L.L.W. Cheung, J.P. Pezacki, Kinugasa Reactions in Water: From Green Chemistry to Bioorthogonal Labelling, Molecules. (2015) 6959–6969.
[31] Y. Volkova, S. Baranin, I. Zavarzin, A3 Coupling Reaction in the Synthesis of Heterocyclic Compounds, Adv. Synth. Catal. 363 (1) (2021) 40–61.
[32] S. Díez-González, Chapter Three - Copper(I)–Acetylides: Access, Structure, and Relevance in Catalysis, in: P.J. Pérez (Ed.), Advances in Organometallic Chemistry, Academic Press, 2016, pp. 93–141.
[33] G. Fang, X. Bi, Silver-catalysed reactions of alkynes: recent advances, Chem. Soc. Rev. 44 (22) (2015) 8124–8173.
[34] T. Tábi, L. Vécsei, M.B. Youdim, P. Riederer, É. Szökő, Selegiline: a molecule with innovative potential, J. Neural Transm. 127 (5) (2020) 831–842.
[35] S. Xie, J. Chen, X. Li, T. Su, Y. Wang, Z. Wang, L. Huang, X. Li, Synthesis and evaluation of selegiline derivatives as monoamine oxidase inhibitor, antioxidant and metal chelator against Alzheimer's disease, Bioorg. Med. Chem. 23 (13) (2015) 3722–3729.
[36] N.B. Kondekar, P. Kumar, Synthesis of (R)-Selegiline via Hydrolytic Kinetic Resolution, Synth. Commun. 41 (9) (2011) 1301–1308.
[37] L.M. Chahine, M.B. Stern, Rasagiline in Parkinson's Disease, in: M.B.H. Youdim, P. Douce (Eds.), International Review of Neurobiology, Academic Press, 2011, pp. 151–168.
[38] I. Denya, S.F. Malan, A.B. Enogieru, S.I. Omoruyi, O.E. Ekpo, E. Kapp, F.T. Zindo, J. Joubert, Design, synthesis and evaluation of indole derivatives as multifunctional agents against Alzheimer's disease, Medchemcomm. 9 (2) (2018) 357–370.
[39] O. Weinreb, T. Amit, O. Bar-Am, M.B.H. Youdim, A novel anti-Alzheimer's disease drug, ladostigil: neuroprotective, multimodal brain-selective monoamine oxidase and cholinesterase inhibitor, in: M.B.H. Youdim, P. Douce (Eds.), A novel anti-Alzheimer's disease drug, ladostigil: neuroprotective, multimodal brain-selective

monoamine oxidase and cholinesterase inhibitor, Int. Rev. Neurobiol. (2011) 191–215.
[40] A. Kumar, M.K. Gangwar, A.P. Prakasham, D. Mhatre, A.C. Kalita, P. Ghosh, Accessing a Biologically Relevant Benzofuran Skeleton by a One-Pot Tandem Heck Alkynylation/Cyclization Reaction Using Well-Defined Palladium N-Heterocyclic Carbene Complexes, Inorg. Chem. 55 (6) (2016) 2882–2893.
[41] C. Singh, A.P. Prakasham, M.K. Gangwar, R.J. Butcher, P. Ghosh, One-Pot Tandem Hiyama Alkynylation/Cyclizations by Palladium(II) Acyclic Diaminocarbene (ADC) Complexes Yielding Biologically Relevant Benzofuran Scaffolds, ACS. Omega 3 (2) (2018) 1740–1756.
[42] C. Singh, A.P. Prakasham, P. Ghosh, Palladium Acyclic Diaminocarbene (ADC) Triflate Complexes as Effective Precatalysts for the Hiyama Alkynylation/Cyclization Reaction Yielding Benzofuran Compounds: Probing the Influence of the Triflate Co-Ligand in the One-Pot Tandem Reaction, ChemistrySelect. 4 (1) (2019) 329–336.
[43] A.P. Prakasham, S. Ta, S. Dey, P. Ghosh, One pot tandem dual C-C and C-O bond reductions in the β-alkylation of secondary alcohols with primary alcohols by ruthenium complexes of amido and picolyl functionalized N-heterocyclic carbenes, Dalton Transactions 50 (43) (2021) 15640–15654.
[44] A. Kumar, S. Ta, C. Nettem, J.M. Tanski, G. Rajaraman, P. Ghosh, One pot tandem dehydrogenative cross-coupling of primary and secondary alcohols by ruthenium amido-functionalized 1,2,4-triazole derived N-heterocyclic carbene complexes, RSC. Adv. 12 (45) (2022) 28961–28984.
[45] S. Dey, P. Ghosh, Accessing Heteroannular Benzoxazole and Benzimidazole Scaffolds via Carbodiimides Using Azide–Isocyanide Cross-Coupling as Catalyzed by Mesoionic Singlet Palladium Carbene Complexes Derived from a Phenothiazine Moiety, ACS. Omega 8 (12) (2023) 11039–11064.
[46] J. Singh, S. Sharma, A.P. Prakasham, G. Rajaraman, P. Ghosh, Accessing Bioactive Hydrazones by the Hydrohydrazination of Terminal Alkynes Catalyzed by Gold(I) Acyclic Aminooxy Carbene Complexes and Their Gold(I) Arylthiolato and Gold(III) Tribromo Derivatives: A Combined Experimental and Computational Study, ACS. Omega 8 (23) (2023) 21042–21073.
[47] S. Ray, R. Mohan, J.K. Singh, M.K. Samantaray, M.M. Shaikh, D. Panda, P. Ghosh, Anticancer and antimicrobial metallopharmaceutical agents based on palladium, gold, and silver N-heterocyclic carbene complexes, J. Am. Chem. Soc. 129 (48) (2007) 15042–15053.
[48] A. Kumar, A. Naaz, A.P. Prakasham, M.K. Gangwar, R.J. Butcher, D. Panda, P. Ghosh, Potent Anticancer Activity with High Selectivity of a Chiral Palladium N-Heterocyclic Carbene Complex, ACS. Omega 2 (8) (2017) 4632–4646.
[49] A. Sorroche, S. Moreno, M. Elena Olmos, M. Monge, J.M. López-de-Luzuriaga, Deciphering the Primary Role of Au··· H– X Hydrogen Bonding in Gold Catalysis, Angewandte Chemie 135 (41) (2023) e202310314.
[50] H. Schmidbaur, H.G. Raubenheimer, L. Dobrzańska, The gold–hydrogen bond, Au–H, and the hydrogen bond to gold, Au··· H–X, Chem. Soc. Rev. 43 (1) (2014) 345–380.
[51] H. Darmandeh, J. Löffler, N.V. Tzouras, B. Dereli, T. Scherpf, K.S. Feichtner, S. Vanden Broeck, K. Van Hecke, M. Saab, C.S.J. Cazin, Au··· H– C Hydrogen Bonds as Design Principle in Gold(I)Catalysis, Angewandte Chemie International Edition 60 (38) (2021) 21014–21024.
[52] J. Handelmann, C.N. Babu, H. Steinert, C. Schwarz, T. Scherpf, A. Kroll, V. H. Gessner, Towards the rational design of ylide-substituted phosphines for gold(I)-catalysis: from inactive to ppm-level catalysis, Chem. Sci. 12 (12) (2021) 4329–4337.
[53] J. Farhi, I.N. Lykakis, G.E. Kostakis, Metal-Catalysed A3 Coupling Methodologies: Classification and Visualisation, Catalysts. (2022).
[54] J. Gil-Rubio, V. Cámara, D. Bautista, J. Vicente, Dinuclear Alkynyl Gold(I) Complexes Containing Bridging N-Heterocyclic Dicarbene Ligands: New Synthetic Routes and Luminescence, Organometallics. 31 (15) (2012) 5414–5426.
[55] A. Gómez-Suárez, S. Dupuy, A.M.Z. Slawin, S.P. Nolan, Zuschrift, Angewandte Chemie 125 (3) (2013) 972–976.
[56] M.C. Blanco, J. Cámara, M.C. Gimeno, P.G. Jones, A. Laguna, J.M. López-de-Luzuriaga, M.E. Olmos, M.D. Villacampa, Luminescent Homo- and Heteropolynuclear Gold Complexes Stabilized by a Unique Acetylide Fragment, Organometallics. 31 (7) (2012) 2597–2605.
[57] A.S.K. Hashmi, T. Lauterbach, P. Nösel, M.H. Vilhelmsen, M. Rudolph, F. Rominger, Dual Gold Catalysis: σ,π-Propyne Acetylide and Hydroxyl-Bridged Digold Complexes as Easy-To-Prepare and Easy-To-Handle Precatalysts, Chemistry – A European Journal 19 (3) (2013) 1058–1065.
[58] J. Vicente, M.T. Chicote, M.D. Abrisqueta, M.C. Ramírez de Arellano, P.G. Jones, M.G. Humphrey, M.P. Cifuentes, M. Samoc, B. Luther-Davies, Syntheses, Structure, and Molecular Cubic Hyperpolarizabilities of Systematically Varied Ethynylgold(I) Complexes, Organometallics. 19 (16) (2000) 2968–2974.
[59] J. Vicente, M.T. Chicote, M.M. Alvarez-Falcón, P.G. Jones, Gold(I) and Silver(I)/Gold(I) Complexes Derived from C6Me4(C⁝CH)2-1,2, Organometallics. 24 (19) (2005) 4666–4675.
[60] J. Vicente, M.T. Chicote, M.D. Abrisqueta, M.M. Alvarez-Falcón, M.C. Ramírez de Arellano, P.G. Jones, New Carbenegold(I) Complexes Synthesized by the "Acac Method, Organometallics. 22 (21) (2003) 4327–4333.
[61] B. Cordero, V. Gomez, A.E. Platero-Prats, M. Reves, J. Echeverria, E. Cremades, F. Barragan, S. Alvarez, Covalent radii revisited, Dalton. Trans. (21) (2008) 2832–2838.
[62] S. Zhu, R. Liang, L. Chen, C. Wang, Y. Ren, H. Jiang, A direct and practical approach for the synthesis of Au(I)-NHC complexes from commercially available imidazolium salts and Au(III) salts, Tetrahedron. Lett. 53 (7) (2012) 815–818.
[63] C. Costabile, A. Mariconda, M. Sirignano, A. Crispini, F. Scarpelli, P. Longo, A green approach for A3-coupling reactions: an experimental and theoretical study on NHC silver and gold catalysts, New Journal of Chemistry 45 (39) (2021) 18509–18517.
[64] M.N. Rao, R. Manne, J.M. Tanski, R. Butcher, P. Ghosh, One pot synthesis of propargylamines by three component amine-aldehyde-acetylene (A3) coupling catalyzed by neutral Ag(I) and Au(I) and cationic Pd(II) and Ni(II) complexes of a pincer N-heterocyclic carbene, Molecular Catalysis 529 (2022) 112515.
[65] R. Ye, A.V. Zhukhovitskiy, R.V. Kazantsev, S.C. Fakra, B.B. Wickemeyer, F.D. Toste, G.A. Somorjai, Supported Au Nanoparticles with N-Heterocyclic Carbene Ligands as Active and Stable Heterogeneous Catalysts for Lactonization, J. Am. Chem. Soc. 140 (11) (2018) 4144–4149.
[66] X. Ling, S. Roland, M.P. Pileni, Supracrystals of N-Heterocyclic Carbene-Coated Au Nanocrystals, Chemistry of Materials 27 (2) (2015) 414–423.
[67] S. Müllegger, W. Schöfberger, M. Rashidi, T. Lengauer, F. Klappenberger, K. Diller, K. Kara, J.V. Barth, E. Rauls, W.G. Schmidt, R. Koch, Preserving Charge and Oxidation State of Au(III) Ions in an Agent-Functionalized Nanocrystal Model System, ACS. Nano 5 (8) (2011) 6480–6486.
[68] F. Vitale, I. Fratoddi, C. Battocchio, E. Piscopiello, L. Tapfer, M.V. Russo, G. Polzonetti, C. Giannini, Mono- and bi-functional arenethiols as surfactants for gold nanoparticles: synthesis and characterization, Nanoscale Res. Lett. 6 (1) (2011) 103.
[69] A. Neshat, M. Afrasi, S. Gilanchi, M. Gholinejad, An Efficient A3 Coupling Catalyst Based on a Silver Complex Bearing N-Heterocyclic Carbene and Homoscorpionate Bis(3-methyl-mercaptoimidazolyl)borate Ligands, ChemistrySelect. 4 (32) (2019) 9268–9273.
[70] M.J. Frisch, G.W. Trucks, H.B. Schlegel, G.E. Scuseria, M.A. Robb, J.R. Cheeseman, G. Scalmani, V. Barone, G.A. Petersson, H. Nakatsuji, X. Li, M. Caricato, A.V. Marenich, J. Bloino, B.G. Janesko, R. Gomperts, B. Mennucci, H.P. Hratchian, J.V. Ortiz, A.F. Izmaylov, J.L. Sonnenberg, Williams, F. Ding, F. Lipparini, F. Egidi, J. Goings, B. Peng, A. Petrone, T. Henderson, D. Ranasinghe, V.G. Zakrzewski, J. Gao, N. Rega, G. Zheng, W. Liang, M. Hada, M. Ehara, K. Toyota, R. Fukuda, J. Hasegawa, M. Ishida, T. Nakajima, Y. Honda, O. Kitao, H. Nakai, T. Vreven, K. Throssell, J.A. Montgomery Jr., J.E. Peralta, F. Ogliaro, M.J. Bearpark, J.J. Heyd, E.N. Brothers, K.N. Kudin, V.N. Staroverov, T.A. Keith, R. Kobayashi, J. Normand, K. Raghavachari, A.P. Rendell, J.C. Burant, S.S. Iyengar, J. Tomasi, M. Cossi, J.M. Millam, M. Klene, C. Adamo, R. Cammi, J.W. Ochterski, R.L. Martin, K. Morokuma, O. Farkas, J.B. Foresman, D.J. Fox, Gaussian 16 Rev. C.01, Wallingford, CT, 2016.
[71] A.D. Becke, Density-functional thermochemistry. V. Systematic optimization of exchange-correlation functionals, J. Chem. Phys. 107 (20) (1997) 8554–8560.
[72] J. Antony, S. Grimme, Density functional theory including dispersion corrections for intermolecular interactions in a large benchmark set of biologically relevant molecules, Physical Chemistry Chemical Physics 8 (45) (2006) 5287–5293.
[73] L.E. Roy, P.J. Hay, R.L. Martin, Revised Basis Sets for the LANL Effective Core Potentials, J. Chem. Theory. Comput. 4 (7) (2008) 1029–1031.
[74] A.V. Mitin, J. Baker, P. Pulay, An improved 6-31 G* basis set for first-row transition metals, J. Chem. Phys. 118 (17) (2003) 7775–7782.
[75] A.D. Becke, Density-functional exchange-energy approximation with correct asymptotic behavior, Physical Review A 38 (6) (1988) 3098–3100.
[76] F. Weigend, R. Ahlrichs, Balanced basis sets of split valence, triple zeta valence and quadruple zeta valence quality for H to Rn: Design and assessment of accuracy, Physical Chemistry Chemical Physics 7 (18) (2005) 3297–3305.
[77] J. Tomasi, B. Mennucci, R. Cammi, Quantum Mechanical Continuum Solvation Models, Chem. Rev. 105 (8) (2005) 2999–3094.
[78] E.D. Glendening, C.R. Landis, F. Weinhold, NBO 6.0: Natural bond orbital analysis program, J. Comput. Chem. 34 (16) (2013) 1429–1437.
[79] F. Neese, Software update: the ORCA program system, version 4.0, Wiley Interdisciplinary Reviews: Computational Molecular Science 8 (1) (2018) e1327.
[80] A. Altun, F. Neese, G. Bistoni, Local energy decomposition analysis of hydrogen-bonded dimers within a domain-based pair natural orbital coupled cluster study, Beilstein. J. Org. Chem. 14 (1) (2018) 919–929.
[81] A. Altun, R. Izsák, G. Bistoni, Local energy decomposition of coupled-cluster interaction energies: Interpretation, benchmarks, and comparison with symmetry-adapted perturbation theory, Int. J. Quantum. Chem. 121 (3) (2021) e26339.
[82] C.A. de Almeida, L.P.N.M. Pinto, H.F. Dos Santos, D.F.S. Paschoal, Vibrational frequencies and intramolecular force constants for cisplatin: assessing the role of the platinum basis set and relativistic effects, J. Mol. Model. 27 (11) (2021) 322.
[83] T. Noro, M. Sekiya, T. Koga, Sapporo-(DKH3)-n ZP (n= D, T, Q) sets for the sixth period s-, d-, and p-block atoms, Theor. Chem. Acc. 132 (2013) 1–5.
[84] L.B. Krivdin, Computational protocols for calculating 13C NMR chemical shifts, Prog. Nucl. Magn. Reson. Spectrosc. 112 (2019) 103–156.
[85] M. Kaupp, O.L. Malkin, V.G. Malkin, Interpretation of 13C NMR chemical shifts in halomethyl cations, On the importance of spin-orbit coupling and electron correlation, Chem. Phys. Lett. 265 (1-2) (1997) 55–59.
[86] H.W.L. Fraser, E.H. Payne, A. Sarkar, L.R.B. Wilson, D. Mitcov, G.S. Nichol, G. Rajaraman, S. Piligkos, E.K. Brechin, [(V IV O) 2 M II5](M= Ni, Co) Anderson wheels, Dalton Transactions 50 (36) (2021) 12495–12501.

[87] D.A. Pantazis, F. Neese, All-Electron Scalar Relativistic Basis Sets for the Actinides, J. Chem. Theory. Comput. 7 (3) (2011) 677–684.
[88] M. Kaupp, Interpretation of NMR Chemical Shifts, Calculation of NMR and EPR Parameters 2004, pp. 293-306.
[89] L. Falivene, R. Credendino, A. Poater, A. Petta, L. Serra, R. Oliva, V. Scarano, L. Cavallo, SambVca 2. A Web Tool for Analyzing Catalytic Pockets with Topographic Steric Maps, Organometallics. 35 (13) (2016) 2286–2293.
[90] I.S. Bushmarinov, A.L. Konstantin, A. Mikhail Yu, Atomic energy in the 'Atoms in Molecules' theory and its use for solving chemical problems, Russian Chemical Reviews 78 (4) (2009) 283.
[91] G. Greczynski, L. Hultman, C 1s Peak of Adventitious Carbon Aligns to the Vacuum Level: Dire Consequences for Material's Bonding Assignment by Photoelectron Spectroscopy, Chemphyschem. 18 (12) (2017) 1507–1512.
[92] A.J. Young, M. Sauer, G.M.D.M. Rubio, A. Sato, A. Foelske, C.J. Serpell, J.M. Chin, M.R. Reithofer, One-step synthesis and XPS investigations of chiral NHC–Au(0)/Au (i) nanoparticles, Nanoscale 11 (17) (2019) 8327–8333.
[93] G.M. Sheldrick, Crystal structure refinement with SHELXL, Acta Crystallogr., Sect. C: Struct. Chem. 71 (1) (2015) 3–8.
[94] D. Demir Atli, B. Şen, Dinuclear silver-bis(N-heterocyclic carbene) complexes: Synthesis, catalytic activity in propargylamine formation and computational studies, J. Coord. Chem. 74 (14) (2021) 2289–2301.
[95] M. Aliaga-Lavrijsen, R.P. Herrera, M.D. Villacampa, M.C. Gimeno, Efficient Gold(I) Acyclic Diaminocarbenes for the Synthesis of Propargylamines and Indolizines, ACS. Omega 3 (8) (2018) 9805–9813.
[96] M.R. Silva-Junior, M. Schreiber, S. Sauer, W. Thiel, Benchmarks of electronically excited states: Basis set effects on CASPT2 results, J. Chem. Phys. 133 (17) (2010).